tetranorprostan-1,20-dioic acid (tetranor PGDM) was shown to be a major urinary metabolite of PGD_2 and to reflect its biosynthesis [13].

2. Materials and methods

2.1. Patients

More than 400 DMD patients were referred to the DMD specialist clinic at Kobe University Hospital (Kobe, Japan). Patients were regularly checked for their clinical findings. The causative mutation in the *dystrophin* gene was identified in each case [1]. When corticosteroid use was indicated, predonine was prescribed at 0.5 mg/kg on alternate days. However, fewer than one fifth of patients received corticosteroid therapy in our clinic. One hundred seventeen DMD patients from 4 to 15 y were enrolled in this study and their first morning urines were obtained at 191 points. Age matched 71 male controls were recruited from healthy relatives or volunteers and first morning urine were obtained at 79 points. Two samplings from 1 patient were done at least 6 months separated. Information concerning the clinical condition of the patients and controls was obtained from their parents and hospital records, respectively. Voluntary urine samples or first morning urine samples were collected. Urine samples were stored at −20 °C until analysis. The protocols used in this study were approved by the ethics committee of Kobe University School of Medicine. All urine analysis was conducted after obtaining informed consent from the patients' parents.

2.2. Measurement of urinary tetranor PGDM concentration using mass spectrometry

The urine samples (0.4 ml) diluted with 0.5 ml of water were acidified by the addition of 1 mol/l HCl (final pH ~ 3) and 50 μl (5 ng) of d6-tetranor PGDM and 9,15-dioxo-11α-hydroxy-,2,3,4,5-tetranorprostan-1,20-dioic acid (tetranor PGEM) (Cayman Chemical, Ann Arbor, MI) was added as an internal standard. The mixtures were purified by solid-phase extraction using Sep-Pak Vac 3 cc cartridges (Waters Corp., Milford, MA). The cartridges were pre-conditioned with 3 ml of ethanol and equilibrated with 3 ml of water. The urine sample was applied to the cartridge, which was washed with 6 ml of 5% (v/v) acetonitrile in and then with 6 ml of n-hexane. The analyte and internal standard were eluted from the cartridge with 3 ml of ethyl acetate. The eluate was collected and dried under vacuum. The resulting residue was reconstituted in 100 μl of 10% (v/v) acetonitrile. The sample solution (20 μl) containing tetranor PGDM and tetranor PGEM was then introduced into an API3000 LC–MS/MS system (Applied Biosystems, Foster City, CA) equipped with an electrospray (Turbospray) interface. The HPLC column was a 150 × 2.1-mm i.d. Inertsil ODS-3 (GL Sciences, Tokyo, Japan). LC separation was carried out using a mobile phase consisting of 0.01% (v/v) acetic acid (solvent A) and acetonitrile (solvent B). The following gradient was employed at a flow rate of 250 μl/min: initial (2 min) at 10:95 (A:B); 24 min at 30:70, 27 min at 70:30. The LC–MS/MS was operated in the negative ion mode. The urinary tetranor PGDM was measured in the selected reaction monitoring mode. The transitions monitored were *m/z* 327–143 for the endogenous material and *m/z* 333–149 for the internal standard. The scan time was 250 ms.

The self-prepared samples were used to document the specificity of this method. The linearity of standard calibration curve was examined by analysis of seven concentrations (0.125, 0.250, 0.625, 1.25, 2.50, 6.25 and 12.5 ng/ml). The limit of quantitation defined as the lowest concentration on the calibration curve could be determined with 75–125% of accuracy and CVs < 20%, and the limit of detection was determined at a S/N of 3. The recovery was obtained by experiments using spiked blank matrix with mutually independent replicates at three concentrations of tPGDM (2.50, 6.25 and 12.5 ng/ml). Ten measurements were performed at each of the above 3 concentrations. The intra-day CV of this method was examined using 10 parallel samples at 3 concentrations (2.50, 6.25 and 12.5 ng/ml) prepared as described above. All samples were analyzed on the same day together with the daily calibration; the accuracy and precision were determined at each concentration. Acceptance criteria defined as precision should not exceed 15%, while accuracy should be within 100 ± 15% at each concentration. Acetonitrile (HPLC grade), ethanol, n-hexane, ethyl acetate, and all other chemicals were from Wako Pure Chemical Industries Ltd. (Osaka, Japan).

2.3. Creatinine measurements

Urinary creatinine concentration was measured using a creatinine measurement kit (Wako Pure Chemical Industries Ltd.).

2.4. Statistical analysis

Group difference between DMD patients and healthy children was analyzed using *t*-tests or 2-way analysis of variance in GraphPad Prism 5 (GraphPad Software, Inc., La Jolla, CA). Statistical significance was set at $p < 0.05$.

3. Results

Tetranor PGDM in urine samples was determined in a selected ion monitoring mode by LC–MS/MS. The monitored product ion peaks of tetranor PGDM and tetranor PGEM were clearly separated in the mass chromatogram with each single peak but no interference peaks. The retention time of these peaks of urine samples matched with that of controls (Fig. 1). The concentration of tetranor PGDM was quantitated

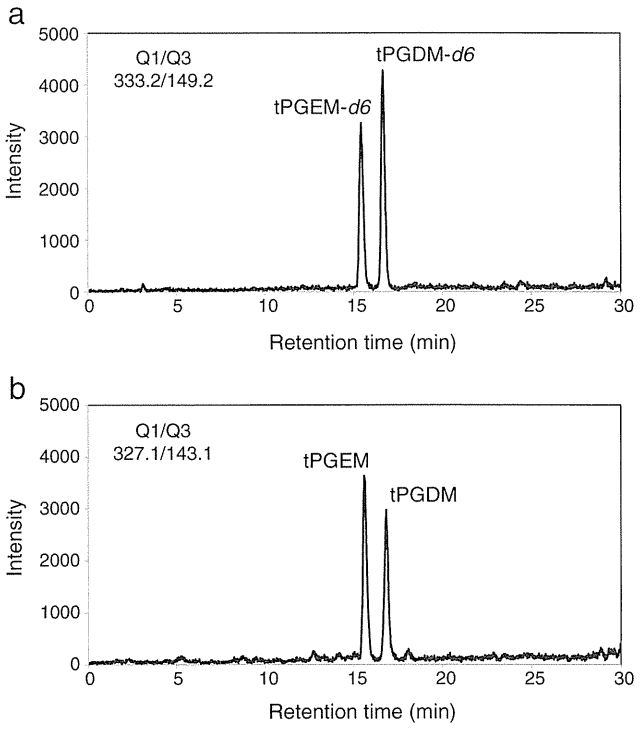

Fig. 1. LC–MS/MS chromatograms. Representative chromatograms of d6-teteranor PGDM and d6-tetranor PGEM (a) and endogenous compounds in urine (b). The first-order MS (Q1) analysis was conducted using negative ion scanning mode to ascertain that the precursor ion peak of d6-tetranor PGDM and tetranor PGDM was $[M-H]^-$ and M-1 of these compounds was 332.2 and 327.1, respectively. The second-order MS (Q2) analysis was done after the collision of precursor ion of the respective PGDM with $[M-H]^-$. Through adjustment of cone voltage and impact energy, the second-order mass chromatogram was obtained, and is shown. The ion transitions (Q1/Q3) of *m/z* 332.2/149.2 and 327.1/143.1 were used to analyze quantitatively and qualitatively, respectively.

using the peak area ratios of tetranor PGDM to d6-tetranor PGDM, on the basis of the calibration curve. The calibration curve was linear in the concentration range of 0.125–12.5 ng/ml (1/x weighting, $y = 0.072x + 0.00503$, $r = 0.997$). The lower limit of quantification reached 0.125 ng/ml. The intra- and the inter-day precision were less than 5.5% and 8.5%, respectively. The current LC–MS/MS method was validated as simple, sensitive, and accurate.

Urinary tetranor PGDM concentrations of DMD patients were determined in samples obtained at voluntary urination. The concentration fluctuated during the day but the first morning urine showed the lowest daytime concentration in all the examined paired samples (data not shown). Therefore, we used the first morning urine for further analyses, as has been suggested for adults [14]. Urine samples were obtained at 191 points from 117 DMD patients aged from 4 to 15 y and 79 points from 71 age-matched healthy children (Fig. 2a). In controls, the concentration of tetranor PGDM was 3.08 ± 0.15 ng/mg creatinine (mean ± SE), with a range of 1.23 to 7.08 ng/mg creatinine. In contrast, the concentration in DMD patients was 6.90 ± 0.35 ng/mg creatinine (range, 0.38 to 26.46 ng/mg creatinine). The mean concentration of tetranor PGDM in DMD patients was approximately 2.2-times higher than that in controls ($p < 0.0001$).

Corticosteroids are administered to DMD patients even though the mechanism of action is unknown [15]. One report suggested that the anti-inflammatory effect of corticosteroids is due to the suppression of prostaglandin-related inflammation [16]. Therefore, we examined whether corticosteroid administration affected the urinary excretion of tetranor PGDM. The average urinary excretion of tetranor PGDM was 5.44 ± 0.81 ($n = 28$) and 7.15 ± 0.38 ($n = 163$) ng/mg creatinine in DMD patients with and without corticosteroid therapy, respectively (Fig. 2b). No significant difference ($p = 0.078$) was found. This indicates that the benefit of our corticosteroid treatment is not observed.

To examine chronological changes, we plotted urinary tetranor PGDM concentrations against the age of the patients (Fig. 3a). The concentration in controls did not change greatly by age. In DMD patients, the tetranor PGDM concentrations were higher at younger ages (4–7 y) than in controls. Remarkably, they surged still higher from age 8 to 9 y, the beginning of the non-ambulant stage, and stayed in high concentration thereafter. Urinary tetranor PGDM was significantly higher in the older age DMD group (age 8–15 y) than in the younger age group (age 4–7 y) (Fig. 3b). In contrast, urinary tetranor PGDM was significantly lower in the older age control group (age 8–15 y) than in the younger age group (age 4–7 y) (Fig. 3b). Our results indicated high production of PGD_2 in DMD patients and suggested a role of PGD_2 in DMD pathology, especially the older DMD patients.

4. Discussion

We established a way to quantitate urinary PGDM using LC–MS/MS without a treatment of urine sample with methoxyamine (Fig. 1). Our quantitation way became suitable for clinical application by avoiding a time- and cost-consuming methoxyamine modification that has been employed [13]. It was found that urinary concentrations of tetranor PGDM were approximately 2.2-times higher in DMD patients than in controls (Fig. 2). Furthermore, it was first shown that urinary tetranor PGDM concentrations in DMD patients chronologically fluctuated (Fig. 2). It was remarkable that concentrations of urinary tetranor PGD_2 increased still further from the age of 8 y. Since the concentration of urinary tetranor PGDM has been reported to reflect the amount of PGD_2 in the body and ultimately reflect the activity of HPGDS [13], our findings indicated high HPGDS activity in the body of DMD patients. Immunohistochemical examination of HPGDS in biopsied skeletal muscle disclosed HPGDS-positive necrotic muscle fibers from DMD patients and myositis patients [12]. However, HPGDS was not stained in skeletal muscles of the control and Fukuyama-type muscular dystrophy [12]. Urinary excretion concentration of tetranor PGDM in DMD patients (Fig. 2) implied a 2.2-times increase in HPGDS. Our findings were also consistent with those of a murine study, in which the urinary concentration of tetranor PGDM was approximately 3-times higher in *mdx* mice than in wild-type mice [16]. This indicates that similar pathogenic mechanisms caused by primary dystrophin deficiency occur in both human and mouse. PGD_2 is considered an important molecule in the pathology of DMD.

Urinary tetranor PGDM has been shown to be increased in adults with inflammatory conditions such as chronic obstructive pulmonary disease, asthma, and amyotrophic lateral sclerosis, and PGD_2 is considered a mediator of inflammation in these conditions [13,14,17,18]. Therefore, increased urinary concentrations of tetranor PGDM in DMD suggested that PGD_2-mediated inflammation plays a role in the pathology of DMD. This finding may pave the way towards understanding the pathogenesis of DMD. However, it was questioned why urinary tetranor PGDM concentration increased by aging. As HPGDS is expressed in necrotic muscle fibers [12], increased urinary PGDM is supposed to relate with abundance of necrotic muscle fibers.

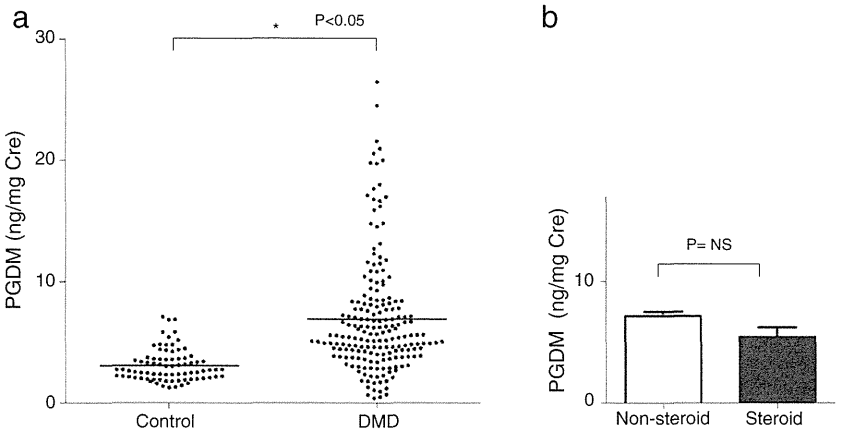

Fig. 2. Urinary tetranor PGDM in DMD patients and healthy children. a. Urinary tetranor PGDM concentration in DMD patients and healthy control children. Individual data points showing urinary tetranor PGDM concentration are represented by circles. In controls, the levels of tetranor PGDM were 3.08 ± 0.15 ng/mg creatinine (mean ± SE) (range, 1.23 to 7.08 ng/mg creatinine), while those were 6.90 ± 0.35 ng/mg creatinine (range, 0.38 to 26.46 ng/mg creatinine) in DMD patients. The mean concentration of tetranor PGDM in DMD patients was approximately 2.2-times higher than that in controls ($p < 0.0001$). The horizontal bars represent the mean. b. Effect of corticosteroid treatment on urinary tetranor PGDM concentration in DMD patients. The average urinary excretion of tetranor PGDM was 5.44 ± 0.81($n = 28$) and 7.15 ± 0.38 ($n = 163$) ng/mg creatinine in DMD patients with (Steroid) and without corticosteroid therapy (Non-steroid), respectively. The data are shown as mean + SE. Bars and horizontal lines represent mean and SE, respectively. There was no significant difference between patients receiving corticosteroid (Steroid) ($n = 28$) or not receiving (Non-steroid) ($n = 163$) corticosteroid treatment.

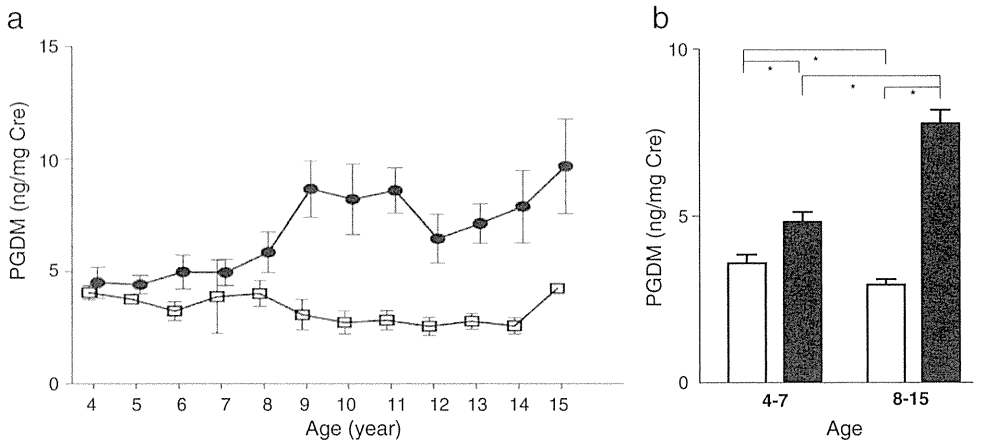

Fig. 3. Chronological changes of urinary tetranor PGDM. a. Chronological changes of mean levels of urinary tetranor PGDM. Mean levels of urinary tetranor PGDM are shown by age in 191 DMD samples (black circles) and 79 control samples (open boxes). The tetranor PGDM levels in DMD patients were higher than controls. Remarkably, they surged still higher from ages 8 to 9, the beginning of the non-ambulant stage, and stayed high level thereafter. However, the tetranor PGDM levels in controls were similar levels throughout the examination period. The data are shown as mean ± SE. b. Comparison of urinary tetranor PGDM concentrations in aged 4 to 7 and 8 to 15 groups. Mean concentration of urinary PGDM in aged 4–7 and 8–15 groups of DMD patients (black columns) and controls (open columns) are shown. In DMD urinary tetranor PGDM was significantly higher in the older age group (age 8–15) ($n = 140$) than in the younger age group (age 4–7) ($n = 51$) (7.69 ± 0.44 vs. 4.75 ± 0.32 ng/mg creatinine (mean ± SE) ($p < 0.05$)). In control, however, urinary tetranor PGDM was significantly lower in the older age group (age 8–15) ($n = 57$) than in the younger age group (age 4–7) ($n = 22$) (2.90 ± 0.17 vs. 3.55 ± 0.30 ng/mg creatinine (mean ± SE) ($p < 0.05$)). The data are represented as mean + SE. Asterisks mean significant difference ($p < 0.05$).

It has been demonstrated that creatinine excretion progressively decreases in parallel with muscle wasting in patients with Duchenne muscular dystrophy [19]. The apparent increase of tetranor PGDM (expressed as ng/mg creatinine) in the DMD patients (Fig. 2) was attributable, at least in part, to the decreased concentrations of creatinine excretion in these patients. Considering that urinary creatinine excretion could be a reliable index of muscle mass [20], urinary tetranor PGDM concentration expressed as ng/mg creatinine was considered to reflect a PGD_2 production in a certain amount of muscle mass. Namely, DMD patients are supposed to have higher HPGDS activity than controls in a certain volume of muscle. Ideally, tetranor PGDM concentrations would have been studied in 24 h urine samples, allowing them also to be expressed as total output per day and hence independent of creatinine concentration. However, it was not considered reasonable to perform 24 h urine collections in this patient population.

HPGDS is widely distributed in various human organs [21]. However, the remarkable increases in HPGDS in DMD boys are observed only in the skeletal muscle [12]. The other type of PGDS, lipocalin-type PGDS, is distributed in the heart, male genital organs, and the central nervous system [22]. Lipocalin-type PGDS is not increased in the DMD muscle. In *mdx* mice, a murine model of DMD, the urinary tetranor PGDM concentration was decreased by administration of an HPGDS inhibitor, HQL-79 [16]. These indicated that urinary tetranor PGDM in DMD is mainly produced by HPGDS-derived PGD_2.

Administration of corticosteroids has been reported to give some benefit to DMD patients [23,24]. The mechanism through which corticosteroids exert their action is still unclear [15]. It has been proposed that corticosteroids alleviate the dystrophy process through immunosuppression and reduction of inflammation [25] or that corticosteroids act directly on muscle fibers by stabilizing sarcolemma [26]. It was reported that corticosteroids suppress the biosynthesis of prostaglandins by suppression of their biosynthesis enzymes including phospholipase A_2 and cyclooxygenase [27]. Therefore, corticosteroids were supposed to decrease urinary tetranor PGDM excretion by suppression of prostaglandin synthesis. However, we found no significant difference in urinary tetranor PGDM concentrations between DMD patients with and without corticosteroid treatment (Fig. 2). This suggested that the benefits of corticosteroid administration are not mediated through PGD_2-related inflammation or that our treatment protocol (0.5 mg/kg on alternative days) is not enough to modulate PGDS. It needs further study to clarify this.

DMD is caused by a deficiency of dystrophin in skeletal muscle. The clinical time-course of DMD is well known [9], but the detailed pathogenesis of the progressive muscle wasting has not been elucidated. Muscle degeneration can be observed before birth [6], but the minimal disability stage occurs between ages 4 and 5 y. Mechanical injury to dystrophin deficient membranes is an important factor promoting dystrophic disease pathology but it does not fully explain DMD disease onset and progression. Aberrant intracellular signaling cascades, which regulate both inflammatory and immune processes, have been considered to contribute substantially to the degenerative process. Observations of upregulated inflammatory genes and activated immune cell infiltrates during critical disease stages in dystrophic muscle suggest that these inflammatory processes may play a critical role in initiating and exacerbating muscle wasting [28–32]. A major limitation in understanding the role of the inflammatory immune response in DMD is the absence of detailed time-course studies before, during, and after the onset of lesion development in the muscles of affected humans. It was remarkable that urinary tetranor PGDM concentrations changed chronologically, with a notable increase from the age of 8 y (Fig. 3a). Our findings are compatible with those of Okinaga et al. who showed HPGDS-positive hyalinated necrotic muscle fibers in all aged DMD patients but not in all younger patients [12]. Taken this into consideration, it was suggested that hyalinated fibers expressing HPGDS increase in skeletal muscles of aged DMD patients.

It has been suggested that cycles of degeneration and regeneration in dystrophic muscle eventually deplete satellite replacement cells (i.e., muscle stem cells) [8,33] and that, once the satellite cells are depleted, muscle regeneration ceases, promoting the progressive replacement of muscle tissue with adipose and fibrous connective tissues [34]. However, the mechanisms regulating the degeneration and regeneration cycles have not been clearly defined [9]. Ages 8 to 9 y when urinary tetranor PGDM surged corresponds to the time when the clinical disability changes from the minimal to the severe disability stage. It was supposed that the surge in production of PGD_2 may relate to this progression. The loss of ambulation was reported to manifest at a mean age of 10.3 y in a recent study on genetically confirmed DMD cases [2]. High plateau concentration of urinary tetranor PGDM corresponded to this non-ambulant stage. Our results suggest that PGD_2-mediated inflammation augments pathophysiology in the advanced stages of DMD. Therefore, chronological changes of urinary tetranor PGDM were considered to reflect clinical progression.

Inhibition of PGD_2 production has been proposed as a target of DMD treatment based on an animal study [16]. Administration of the HPGDS inhibitor HQL-79 was shown to decrease urinary tetranor PGDM concentrations and ameliorate muscle necrosis in *mdx* mice, DMD model mice [16]. Our results showing high production of PGD_2 in DMD provide a rationale for the administration of an HPGDS inhibitor to DMD patients. Recently, a cyclooxygenase inhibitor was shown to be effective in slowing the progression of muscular dystrophy in α-sarcoglycan-null mice [35]. Considering that PGD_2 is synthesized from PGH_2, a product of arachidonic acid generated by cyclooxygenase, inhibition of cyclooxygenase is another choice for the suppression of PGH_2, leading to a decrease in PGD_2. Aspirin has been shown to decrease urinary tetranor PGDM concentrations significantly [16], and to ameliorate muscle morphology in *mdx* mice [36]. So this common drug may also be useful for the treatment of DMD.

5. Conclusion

Urinary tetranor PGDM concentrations were increased in DMD patients and became higher with advancing age. It was indicated that PGD_2-mediated inflammation plays a role in the pathology of DMD. It was supposed that hyalinated fibers expressing HPGDS increase in older DMD patients.

List of abbreviations

DMD Duchenne muscular dystrophy
PG prostaglandin
HPGDS hematopoietic prostaglandin D synthase
tetranor PGDM 11,15-dioxo-9α-hydroxy-,2,3,4,5-tetranorprostan-1,20-dioic acid
tetranor PGEM 9,15-dioxo-11α-hydroxy-,2,3,4,5-tetranorprostan-1,20-dioic acid.

Acknowledgments

We thank all the participating families and the Happy Smile Club. We are grateful to Drs. Shinya Kamauchi and Kousuke Aritake (Department of Molecular Behavioral Biology, Osaka Bioscience Institute, Suita, Osaka, Japan) for their valuable suggestions. This work was supported by a Grant-in-Aid for Scientific Research (B), and a Grant-in-Aid for Exploratory Research from the Japan Society for the Promotion of Science, a Health and Labour Sciences Research Grant for Research on Psychiatric and Neurological Diseases and Mental Health, and a research grant for Nervous and Mental Disorders from the Ministry of Health, Labour, and Welfare, Japan.

References

[1] Takeshima Y, Yagi M, Okizuka Y, et al. Mutation spectrum of the dystrophin gene in 442 Duchenne/Becker muscular dystrophy cases from one Japanese referral center. J Hum Genet 2010;55:379–88.
[2] Magri F, Govoni A, D'Angelo MG, et al. Genotype and phenotype characterization in a large dystrophinopathic cohort with extended follow-up. J Neurol 2011;258:1610–23.
[3] Nishiyama A, Takeshima Y, Zhang Z, et al. Dystrophin nonsense mutations can generate alternative rescue transcripts in lymphocytes. Ann Hum Genet 2008;72:717–24.
[4] Desguerre I, Christov C, Mayer M, et al. Clinical heterogeneity of Duchenne muscular dystrophy (DMD): definition of sub-phenotypes and predictive criteria by long-term follow-up. PLoS One 2009;4:e4347.
[5] Sifringer M, Uhlenberg B, Lammel S, et al. Identification of transcripts from a subtraction library which might be responsible for the mild phenotype in an intrafamilially variable course of Duchenne muscular dystrophy. Hum Genet 2004;114:149–56.
[6] Brooke MH, Fenichel GM, Griggs RC, et al. Clinical investigation in Duchenne dystrophy: 2. Determination of the "power" of therapeutic trials based on the natural history. Muscle Nerve 1983;6:91–103.
[7] Mendell JR, Province MA, Moxley III RT, et al. Clinical investigation of Duchenne muscular dystrophy. A methodology for therapeutic trials based on natural history controls. Arch Neurol 1987;44:808–11.
[8] Bell CD, Conen PE. Histopathological changes in Duchenne muscular dystrophy. J Neurol Sci 1968;7:529–44.
[9] Evans NP, Misyak SA, Robertson JL, Bassaganya-Riera J, Grange RW. Dysregulated intracellular signaling and inflammatory gene expression during initial disease onset in Duchenne muscular dystrophy. Am J Phys Med Rehabil 2009;88:502–22.
[10] Urade Y, Ujihara M, Horiguchi Y, et al. Mast cells contain spleen-type prostaglandin D synthetase. J Biol Chem 1990;265:371–5.
[11] Urade Y, Hayaishi O. Prostaglandin D synthase: structure and function. Vitam Horm 2000;58:89–120.
[12] Okinaga T, Mohri I, Fujimura H, et al. Induction of hematopoietic prostaglandin D synthase in hyalinated necrotic muscle fibers: its implication in grouped necrosis. Acta Neuropathol 2002;104:377–84.
[13] Song WL, Wang M, Ricciotti E, et al. Tetranor PGDM, an abundant urinary metabolite reflects biosynthesis of prostaglandin D2 in mice and humans. J Biol Chem 2008;283:1179–88.
[14] Shinozawa T, Urade Y, Maruyama T, Watabe D. Tetranor PGDM analyses for the amyotrophic lateral sclerosis: positive and simple diagnosis and evaluation of drug effect. Biochem Biophys Res Commun 2011;415:539–44.
[15] Moxley III RT, Pandya S, Ciafaloni E, Fox DJ, Campbell K. Change in natural history of Duchenne muscular dystrophy with long-term corticosteroid treatment: implications for management. J Child Neurol 2010;25:1116–29.
[16] Mohri I, Aritake K, Taniguchi H, et al. Inhibition of prostaglandin D synthase suppresses muscular necrosis. Am J Pathol 2009;174:1735–44.
[17] Zhang Y, Zhang G, Clarke PA, et al. Simultaneous and high-throughput quantitation of urinary tetranor PGDM and tetranor PGEM by online SPE-LC–MS/MS as inflammatory biomarkers. J Mass Spectrom 2011;46:705–11.
[18] Higashi N, Mita H, Yamaguchi H, Fukutomi Y, Akiyama K, Taniguchi M. Urinary tetranor-PGDM concentrations in aspirin-intolerant asthma and anaphylaxis. J Allergy Clin Immunol 2012;129:557–9.
[19] Griggs RC, Forbes G, Moxley RT, Herr BE. The assessment of muscle mass in progressive neuromuscular disease. Neurology 1983;33:158–65.
[20] Wang ZM, Gallagher D, Nelson ME, Matthews DE, Heymsfield SB. Total-body skeletal muscle mass: evaluation of 24-h urinary creatinine excretion by computerized axial tomography. Am J Clin Nutr 1996;63:863–9.
[21] Kanaoka Y, Fujimori K, Kikuno R, Sakaguchi Y, Urade Y, Hayaishi O. Structure and chromosomal localization of human and mouse genes for hematopoietic prostaglandin D synthase. Conservation of the ancestral genomic structure of sigma-class glutathione S-transferase. Eur J Biochem 2000;267:3315–22.
[22] Smith WL, Urade Y, Jakobsson PJ. Enzymes of the cyclooxygenase pathways of prostanoid biosynthesis. Chem Rev 2011;111:5821–65.
[23] Manzur AY, Kuntzer T, Pike M, Swan A. Glucocorticoid corticosteroids for Duchenne muscular dystrophy.Cochrane Database Syst Rev 2008(1) [CD003725].
[24] Escolar DM, Hache LP, Clemens PR, et al. Randomized, blinded trial of weekend vs daily prednisone in Duchenne muscular dystrophy. Neurology 2011;77:444–52.
[25] Iannitti T, Capone S, Feder D, Palmieri B. Clinical use of immunosuppressants in Duchenne muscular dystrophy. J Clin Neuromuscul Dis 2010;12:1–21.
[26] Jacobs SC, Bootsma AL, Willems PW, Bar PR, Wokke JH. Prednisone can protect against exercise-induced muscle damage. J Neurol 1996;243:410–6.
[27] Masferrer JL, Seibert K, Zweifel B, Needleman P. Endogenous glucocorticoids regulate an inducible cyclooxygenase enzyme. Proc Natl Acad Sci U S A 1992;89:3917–21.
[28] Spencer MJ, Montecino-Rodriguez E, Dorshkind K, Tidball JG. Helper (CD4(+)) and cytotoxic (CD8(+)) T cells promote the pathology of dystrophin-deficient muscle. Clin Immunol 2001;98:235–43.
[29] Porter JD, Merriam AP, Leahy P, Gong B, Khanna S. Dissection of temporal gene expression signatures of affected and spared muscle groups in dystrophin-deficient (mdx) mice. Hum Mol Genet 2003;12:1813–21.
[30] Chen YW, Nagaraju K, Bakay M, et al. Early onset of inflammation and later involvement of TGFbeta in Duchenne muscular dystrophy. Neurology 2005;65:826–34.
[31] Pescatori M, Broccolini A, Minetti C, et al. Gene expression profiling in the early phases of DMD: a constant molecular signature characterizes DMD muscle from early postnatal life throughout disease progression. FASEB J 2007;21:1210–26.
[32] Lawler JM. Exacerbation of pathology by oxidative stress in respiratory and locomotor muscles with Duchenne muscular dystrophy. J Physiol 2011;589:2161–70.
[33] Webster C, Silberstein L, Hays AP, Blau HM. Fast muscle fibers are preferentially affected in Duchenne muscular dystrophy. Cell 1988;52:503–13.
[34] Collins CA, Morgan JE. Duchenne's muscular dystrophy: animal models used to investigate pathogenesis and develop therapeutic strategies. Int J Exp Pathol 2003;84:165–72.
[35] Sciorati C, Miglietta D, Buono R, et al. A dual acting compound releasing nitric oxide (NO) and ibuprofen, NCX 320, shows significant therapeutic effects in a mouse model of muscular dystrophy. Pharmacol Res 2011;64:210–7.
[36] Serra F, Quarta M, Canato M, et al. Inflammation in muscular dystrophy and the beneficial effects of non-steroidal anti-inflammatory drugs. Muscle Nerve 2012;46:773–84.

nature immunology

Mast cell maturation is driven via a group III phospholipase A_2-prostaglandin D_2–DP1 receptor paracrine axis

Yoshitaka Taketomi[1,2], Noriko Ueno[1], Takumi Kojima[1], Hiroyasu Sato[1,2], Remi Murase[1,2], Kei Yamamoto[1], Satoshi Tanaka[3], Mariko Sakanaka[4], Masanori Nakamura[5], Yasumasa Nishito[6], Momoko Kawana[2], Naotomo Kambe[7], Kazutaka Ikeda[8], Ryo Taguchi[9], Satoshi Nakamizo[10], Kenji Kabashima[10], Michael H Gelb[11], Makoto Arita[12], Takehiko Yokomizo[13], Motonao Nakamura[14], Kikuko Watanabe[15], Hiroyuki Hirai[16], Masataka Nakamura[17], Yoshimichi Okayama[18], Chisei Ra[18], Kosuke Aritake[19], Yoshihiro Urade[19], Kazushi Morimoto[20], Yukihiko Sugimoto[20], Takao Shimizu[14], Shuh Narumiya[21], Shuntaro Hara[2] & Makoto Murakami[1]

Microenvironment-based alterations in phenotypes of mast cells influence the susceptibility to anaphylaxis, yet the mechanisms underlying proper maturation of mast cells toward an anaphylaxis-sensitive phenotype are incompletely understood. Here we report that PLA2G3, a mammalian homolog of anaphylactic bee venom phospholipase A_2, regulates this process. PLA2G3 secreted from mast cells is coupled with fibroblastic lipocalin-type PGD_2 synthase (L-PGDS) to provide PGD_2, which facilitates mast-cell maturation via PGD_2 receptor DP1. Mice lacking PLA2G3, L-PGDS or DP1, mast cell–deficient mice reconstituted with PLA2G3-null or DP1-null mast cells, or mast cells cultured with L-PGDS–ablated fibroblasts exhibited impaired maturation and anaphylaxis of mast cells. Thus, we describe a lipid-driven PLA2G3–L-PGDS–DP1 loop that drives mast cell maturation.

Anaphylaxis is a serious immediate allergic reaction that involves the activation of mast cells. Cross-linking of the high-affinity IgE receptor FcεRI on mast cells with IgE and antigen initiates signals leading to the release of allergic mediators that induce immediate hypersensitivity[1]. Anaphylaxis is triggered by allergens (for example, insect venom, food and medication) and damages multiple organs including the respiratory and circulatory systems, often leading to life-threatening episodes.

Environmentally induced alterations in phenotypes of mast cells could be one factor that influences the severity of anaphylaxis. Current evidence has established the essential role of stem cell factor (SCF) and its receptor c-Kit (CD117) for development of mast cells[2]. However, the SCF–c-Kit system alone is insufficient to drive the maturation of mast cells fully, as culture of immature mast cells with fibroblasts, but not with SCF alone, can induce differentiation into mature mast cells[2]. Although several cytokines, chemokines and adhesion molecules have supporting roles in tissue-specific homing, growth or differentiation of mast cells[3–7], precise mechanisms underlying mast cell–fibroblast communication leading to optimal maturation of mast cells still remain elusive.

Lipid mediators, such as prostaglandins, leukotrienes and lysophospholipids, have important roles in various biological processes, including allergy[8–15]. A given lipid mediator (for example, PGD_2) aggravates, suppresses or resolves allergic responses[11–13], and this functional variability may depend on the use of distinct biosynthetic enzyme and/or receptor subtypes in different cells. Eicosanoid biosynthesis is initiated by release of arachidonic acid from phospholipids by phospholipase A_2 (PLA_2) enzymes[16]. PLA2G4A (cytosolic PLA_2; $cPLA_2\alpha$) has an essential role in the generation of eicosanoids in various cells, and its deletion results in diminished airway hypersensitivity[17].

[1]Lipid Metabolism Project, Tokyo Metropolitan Institute of Medical Science, Tokyo, Japan. [2]School of Pharmacy, Showa University, Tokyo, Japan. [3]Department of Immunobiology, Okayama University Graduate School of Medicine, Dentistry and Pharmaceutical Sciences, Okayama, Japan. [4]School of Pharmacy and Pharmaceutical Sciences, Mukogawa Women's University, Hyogo, Japan. [5]School of Dentistry, Showa University, Tokyo, Japan. [6]Core Technology and Research Center, Tokyo Metropolitan Institute of Medical Science, Tokyo, Japan. [7]Department of Dermatology, Chiba University Graduate School of Medicine, Chiba, Japan. [8]Institute for Advanced Biosciences, Keio University, Yamagata, Japan. [9]College of Life and Health Sciences, Chubu University, Aichi, Japan. [10]Department of Dermatology, Kyoto University Graduate School of Medicine, Kyoto, Japan. [11]Departments of Chemistry and Biochemistry, University of Washington, Washington, USA. [12]Graduate School of Pharmaceutical Sciences, The University of Tokyo, Tokyo, Japan. [13]Department of Biochemistry, Juntendo University School of Medicine, Tokyo, Japan. [14]Faculty of Medicine, The University of Tokyo, Tokyo, Japan. [15]Department of Nutrition, Koshien University, Hyogo, Japan. [16]Department of Advanced Medicine and Development, Bio Medical Laboratories, Saitama, Japan. [17]Human Gene Sciences Center, Tokyo Medical and Dental University, Tokyo, Japan. [18]Division of Molecular Cell Immunology and Allergology, Advanced Medical Research Center, Nihon University Graduate School of Medical Science, Tokyo, Japan. [19]Department of Molecular Bihavioral Biology, Osaka Bioscience Institute, Osaka, Japan. [20]Department of Pharmaceutical Biochemistry, Graduate School of Medicine and Pharmaceutical Sciences, Kumamoto University, Kumamoto, Japan. [21]Department of Pharmacology, Kyoto University Graduate School of Medicine, Kyoto, Japan. Correspondence should be addressed to M.M. (murakami-mk@igakuken.or.jp).

Received 19 September 2012; accepted 11 March 2013; published online 28 April 2013; doi:10.1038/ni.2586

By contrast, the role of secreted PLA_2 ($sPLA_2$) enzymes is still a subject of debate. Although the lower asthmatic responses in mice lacking two classical $sPLA_2$ enzymes (PLA2G5 and PLA2G10) have revealed their contribution to asthma[18,19], the mechanisms underlying the actions of these enzymes remain poorly understood.

A major bee venom component responsible for anaphylaxis is an atypical form of $sPLA_2$ called BV-PLA_2[20,21]. The mammalian genome encodes group III $sPLA_2$ (PLA2G3), which is the sole homolog of BV-PLA_2[16,22–26]. Here we provide evidence that PLA2G3 is a major mast cell granule-associated $sPLA_2$ that facilitates the maturation of mast cells by driving a previously unrecognized lipid mediator circuit. PLA2G3 released from mast cells is coupled with fibroblast lipocalin-type PGD synthase (L-PGDS) to provide PGD_2, which then acts on type-1 PGD receptor, DP1, induced on mast cells to promote their maturation.

RESULTS

PLA2G3 is expressed in mast cells and induces their activation

When injected intradermally into the mouse ear pinnas, BV-PLA_2 or human PLA2G3 alone induced a similar, dose-dependent vascular leak and augmented passive cutaneous anaphylaxis (PCA) induced by IgE and antigen in $Kit^{+/+}$ mice but not in mast cell–deficient $Kit^{W\text{-}sh/W\text{-}sh}$ mice, in which the SCF receptor c-Kit has a substitution (**Fig. 1a,b**). The edema induced by PLA2G3 was accompanied by ultrastructural degranulation of dermal mast cells (**Fig. 1c**). PLA2G3 induced the release of histamine (**Fig. 1d**), but not of lactate dehydrogenase (**Supplementary Fig. 1a**), from mouse peritoneal mast cells (pMCs) in a Ca^{2+}-dependent manner, indicating that PLA2G3 elicits degranulation, not cell lysis.

Immunohistochemistry analysis revealed that PLA2G3 localized with toluidine blue$^+$ dermal mast cells in wild-type mice but not in $Pla2g3^{-/-}$ mice[22] (**Fig. 1e**). Punctate staining in resting mast cells and sparse staining in degranulated mast cells suggest that PLA2G3 is released upon degranulation (**Fig. 1e,f**). In bone marrow–derived cell populations, *Pla2g3* mRNA was more highly enriched in IL-3–driven bone marrow–derived mast cells (BMMCs) and thymic stromal lymphopoietin (TSLP)-driven bone marrow–derived basophils (BM basophils) than in GM-CSF–driven bone marrow–derived dendritic cells (BMDCs) and M-CSF–driven bone marrow–derived macrophages (BMDMs), and was undetectable in Swiss 3T3 fibroblasts (**Fig. 1g** and **Supplementary Fig. 1b**). Of the mRNAs encoding $sPLA_2$ isoforms, *Pla2g3* mRNA was expressed most abundantly in BMMCs, followed by *Pla2g5* and *Pla2g2e*, whereas mRNAs encoding the other $sPLA_2$ isoforms were undetectable, and SCF-fibroblast–driven maturation of these cells toward connective tissue mast cells (CTMCs) did not affect the expression of these $sPLA_2$ enzymes (**Supplementary Fig. 1c**). When we transfected rat mastocytoma RBL-2H3 cells with cDNA encoding PLA2G3 or a catalytically inactive PLA2G3 variant, III-HQ, in which the catalytic-center histidine was replaced with asparagine[23], release of β-hexosaminidase (β-HEX) and generation of PGD_2 induced by crosslinking of FcεRI by IgE and antigen (hereafter called IgE-Ag) was augmented in cells overexpressing native PLA2G3 but not catalytically inactive PLA2G3 (**Supplementary Fig. 1d**). Thus, PLA2G3 is the main $sPLA_2$ in mouse mast cells, is released by exocytosis and can augment activation of mast cells in a manner dependent upon its enzymatic activity.

Pla2g3 deletion ameliorates mast cell–associated anaphylaxis

Upon passive systemic anaphylaxis (PSA) induced by IgE-Ag, $Pla2g3^{+/+}$ and WBB6F1-$Kit^{+/+}$ mice, but not mast cell–deficient WBB6F1-$Kit^{W/W\text{-}v}$ mice, had much more plasma histamine and a temporary decrease in rectal temperature after systemic antigen challenge, whereas these responses were mild in $Pla2g3^{-/-}$ mice (**Fig. 2a**). Upon PCA induced by IgE-Ag (**Fig. 2b** and **Supplementary Fig. 1e**) or compound 48/80 (C48/80; **Fig. 2c**), edema was markedly lower in $Pla2g3^{-/-}$ mice than $Pla2g3^{+/+}$ mice. By contrast, transgenic overexpression of human

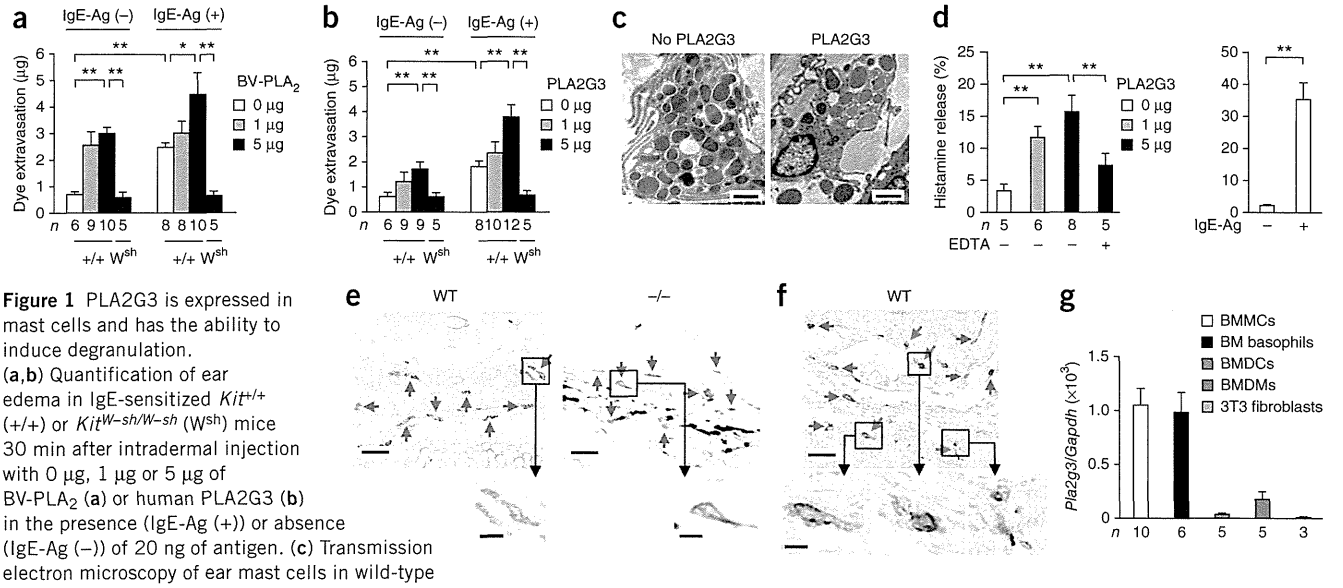

Figure 1 PLA2G3 is expressed in mast cells and has the ability to induce degranulation. (**a**,**b**) Quantification of ear edema in IgE-sensitized $Kit^{+/+}$ (+/+) or $Kit^{W\text{-}sh/W\text{-}sh}$ (W^{sh}) mice 30 min after intradermal injection with 0 μg, 1 μg or 5 μg of BV-PLA_2 (**a**) or human PLA2G3 (**b**) in the presence (IgE-Ag (+)) or absence (IgE-Ag (–)) of 20 ng of antigen. (**c**) Transmission electron microscopy of ear mast cells in wild-type mice with (+) or without (–) administration of 5 μg of PLA2G3. Scale bars, 2 μm. (**d**) Histamine release from wild-type mouse peritoneal cells after treatment for 30 min with 0 μg, 1 μg or 5 μg of PLA2G3 in the presence or absence of 2 mM EDTA (left). Histamine release by IgE-Ag stimulation (positive control) is also shown (right). (**e**,**f**) Immunohistochemistry analysis of ear-skin sections of wild-type (WT) or $Pla2g3^{-/-}$ (–/–) mice before (**e**) and 2 min after (**f**) stimulation with IgE-Ag with anti-PLA2G3 (α-PLA2G3), followed by counterstaining with toluidine blue (scale bars, 50 μm). Boxed areas are magnified below (scale bars, 5 μm). Blue and red arrows indicate resting and degranulated mast cells, respectively. (**g**) Real-time PCR of *Pla2g3* relative to *Gapdh* in indicated bone marrow–derived cells from wild-type mice and Swiss 3T3 fibroblasts. Data are from one experiment (**g**), and compiled from two (**d**) and three (**a**,**b**) experiments (mean ± s.e.m.; $*P < 0.05$ and $**P < 0.01$). Data in **c**,**e**,**f** are representative of two experiments.

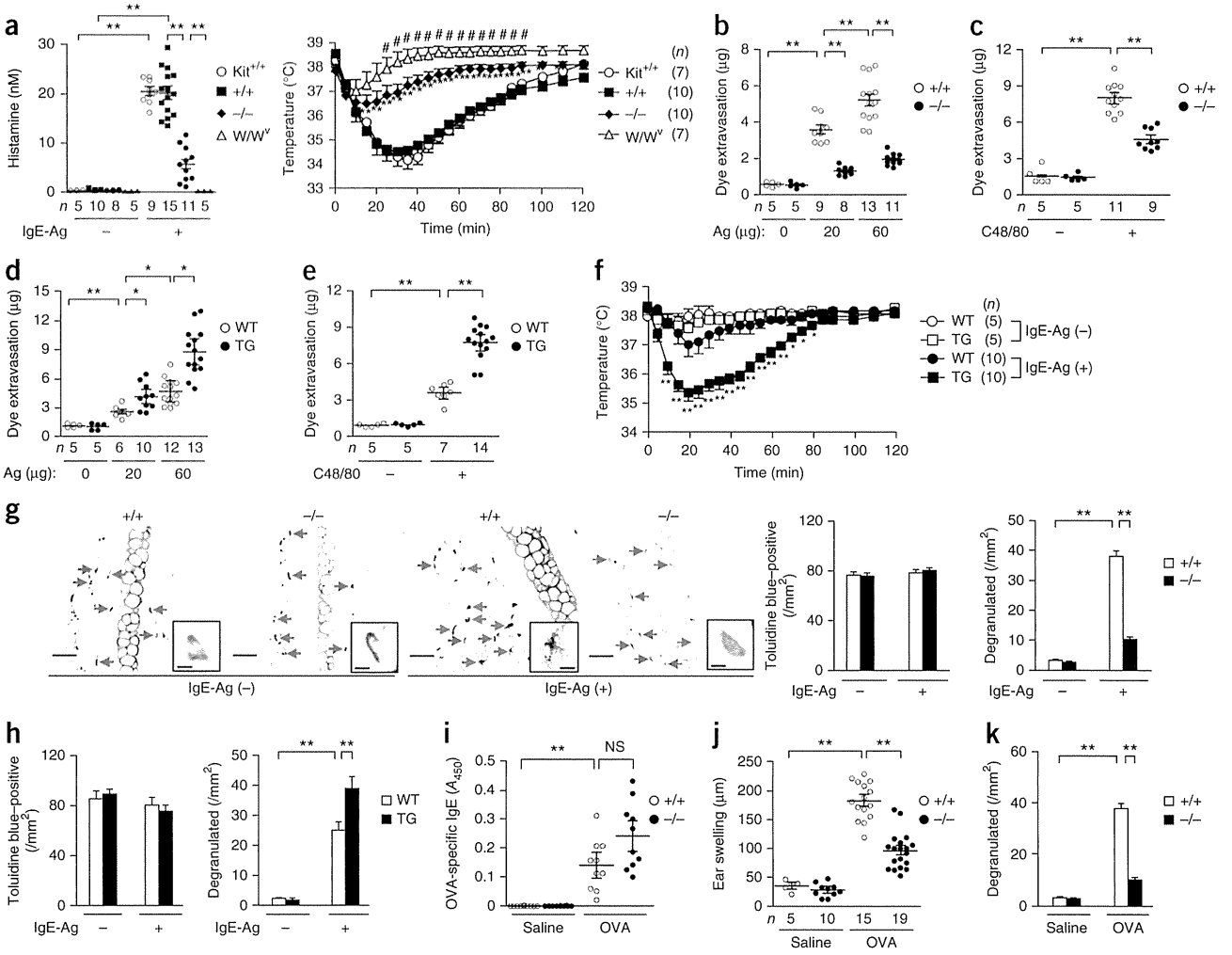

Figure 2 Altered anaphylaxis in mice with deletion or overexpression of PLA2G3. (**a**) Serum histamine concentrations (left) and rectal temperatures (right) in IgE-Ag–dependent PSA in *Pla2g3*$^{+/+}$ (+/+), *Pla2g3*$^{-/-}$ (–/–), WBB6F1-*Kit*$^{+/+}$ (Kit$^{+/+}$) and WBB6F1-*Kit*$^{W/W-v}$ (W/W^{v}) mice after challenge with 500 μg of antigen (Ag). $*P < 0.05$ and $**P < 0.01$, *Pla2g3*$^{-/-}$ versus *Pla2g3*$^{+/+}$ mice and $\#P < 0.05$, *Kit*$^{W/W-v}$ versus *Pla2g3*$^{-/-}$ mice (right). (**b**–**e**) Analysis of ear edema in IgE-Ag–induced (**b**,**d**) or C48/80–induced (**c**,**e**) PCA in *Pla2g3*$^{+/+}$ (+/+) and *Pla2g3*$^{-/-}$ (–/–) mice (**b**,**c**) or wild-type (WT) and *PLA2G3*$^{tg/+}$ (TG) mice (**d**,**e**). (**f**) Rectal temperatures in IgE-Ag–dependent PSA in wild-type (WT) and *PLA2G3*$^{tg/+}$ (TG) mice after challenge with antigen (25 μg). $*P < 0.05$ and $**P < 0.01$, WT versus TG after antigen challenge. (**g**,**h**) Toluidine blue staining of skin sections (left) and counts of toluidine blue^{+} total and degranulated dermal mast cells (right) in *Pla2g3*$^{+/+}$ (+/+) and *Pla2g3*$^{-/-}$ (–/–) mice (**g**) or wild-type (WT) and *PLA2G3*$^{tg/+}$ (TG) mice (**h**) before (IgE-Ag (–)) and 2 min after (IgE-Ag (+)) IgE-Ag–mediated PCA (scale bars, 50 μm) ($n = 6$). Blue and red arrows indicate resting and degranulated mast cells, respectively (**g**). Insets, magnified images (scale bars, 5 μm) (**g**). (**i**–**k**) Serum levels of OVA-specific IgE ($n = 10$; **i**), ear swelling (**j**) and numbers of degranulated ear mast cells ($n = 6$; **k**) in OVA-induced active cutaneous anaphylaxis in *Pla2g3*$^{+/+}$ (+/+) and *Pla2g3*$^{-/-}$ (–/–) mice. Data are from one experiment (**f**–**i**,**k**) and compiled from three experiments (**a**–**e**,**j**) (mean ± s.e.m., $*P < 0.05$; $**P < 0.01$; NS, not significant).

PLA2G3 (*PLA2G3*$^{tg/+}$)[26] augmented both IgE-Ag–dependent (**Fig. 2d** and **Supplementary Fig. 1e**) and C48/80-induced (**Fig. 2e**) PCA as well as IgE-Ag–induced PSA (**Fig. 2f**). Although the ear skin of *Pla2g3*$^{-/-}$ and *Pla2g3*$^{+/+}$ mice contained an equivalent number of toluidine blue^{+} mast cells, we detected fewer cells showing signs of IgE-Ag–induced degranulation in *Pla2g3*$^{-/-}$ mice than in *Pla2g3*$^{+/+}$ mice (**Fig. 2g**). Conversely, ears of IgE-Ag–treated *PLA2G3*$^{tg/+}$ mice had more degranulated mast cells than those of replicate control mice despite a similar total mast cell count (**Fig. 2h**). IgE-Ag–induced PCA in mice lacking other sPLA$_2$ enzymes (*Pla2g2d*$^{-/-}$, *Pla2g2e*$^{-/-}$, *Pla2g2f*$^{-/-}$, *Pla2g5*$^{-/-}$ and *Pla2g10*$^{-/-}$) was similar to that in respective wild-type littermates (**Supplementary Fig. 1f**).

We immunized *Pla2g3*$^{+/+}$ and *Pla2g3*$^{-/-}$ mice intraperitoneally with alum-adsorbed ovalbumin (OVA) and elicited active cutaneous anaphylaxis by intradermal injection of OVA, which cross-links endogenous IgE-bound FcεRI on mast cells. Under conditions in which serum anti-OVA IgE levels were similar in both genotypes, *Pla2g3*$^{-/-}$ mice exhibited lower local anaphylaxis than did *Pla2g3*$^{+/+}$ mice, as indicated by notable reductions in ear swelling and mast cell degranulation (**Fig. 2i–k**). Thus, PLA2G3 is the sole sPLA$_2$ isoform associated with mast cell–dependent anaphylaxis.

Pla2g3 deletion impairs maturation of tissue mast cells

Transmission electron microscopy analysis revealed that resting mast cells in *Pla2g3*$^{+/+}$ mice were oval with regular short processes and had many secretory granules filled with electron-lucent and dense contents, whereas those in *Pla2g3*$^{-/-}$ mice had unusual granules that were small and irregular in size, suggesting the

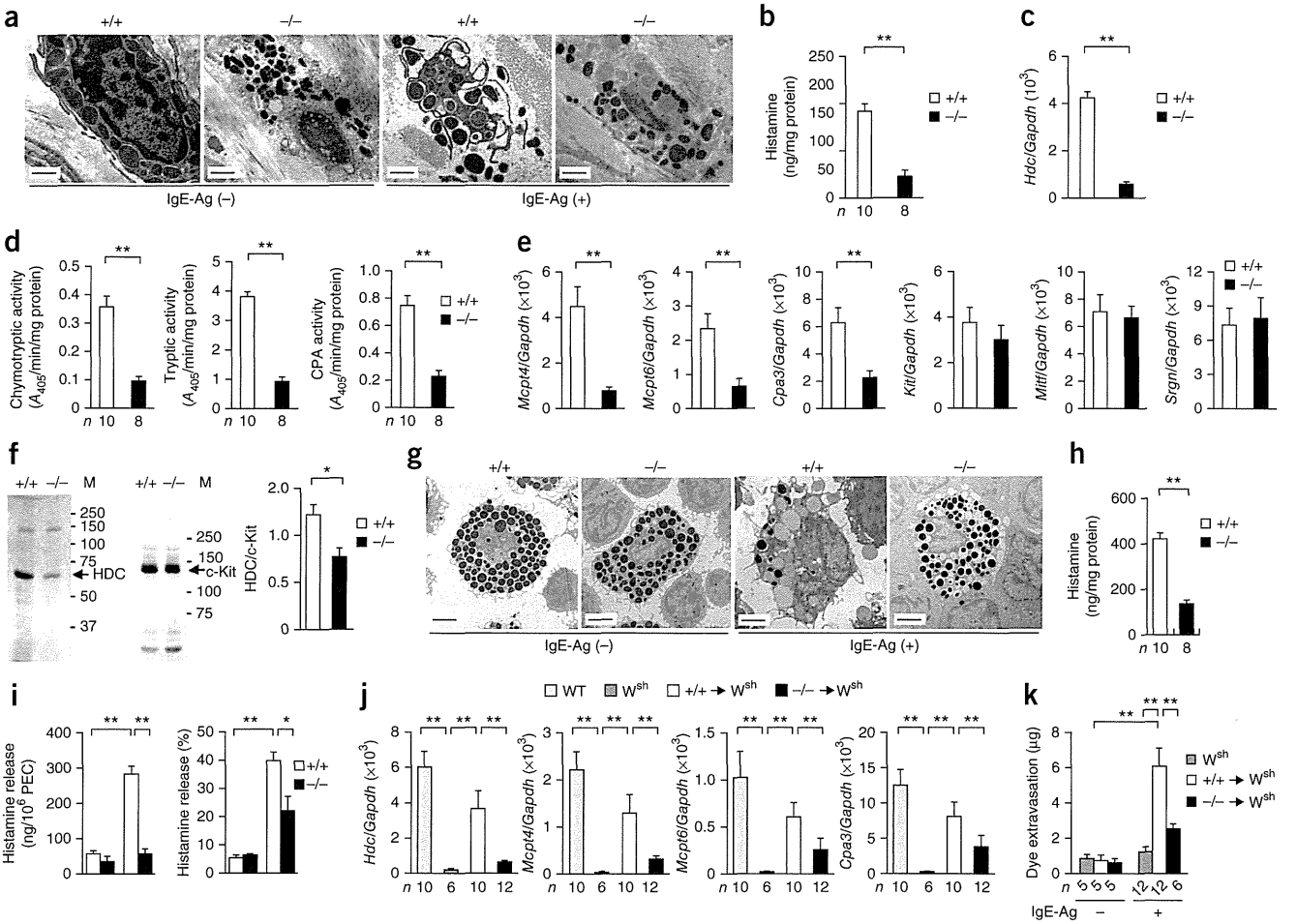

Figure 3 Immature properties of tissue mast cells in *Pla2g3*-deficient mice. (**a**) Transmission electron micrographs of ear mast cells in $Pla2g3^{+/+}$ (+/+) and $Pla2g3^{-/-}$ (−/−) mice before (IgE-Ag (−)) and 2 min after (IgE-Ag (+)) antigen (Ag) challenge. Scale bars, 2 μm. (**b**,**c**) Quantification of histamine amounts (**b**) and *Hdc* mRNA expression relative to that of *Gapdh* ($n = 12$; **c**) in ears of $Pla2g3^{+/+}$ (+/+) and $Pla2g3^{-/-}$ (−/−) mice. (**d**,**e**) Quantification of protease activity (**d**) and mRNA expression of mast cell proteases ($n = 12$) and other mast-cell markers ($n = 7$) (**e**) in ears of $Pla2g3^{+/+}$ (+/+) and $Pla2g3^{-/-}$ (−/−) mice. (**f**) Immunoblotting of HDC and c-Kit in ears of $Pla2g3^{+/+}$ (+/+) and $Pla2g3^{-/-}$ (−/−) mice. M, molecular mass (kDa). The ratio of HDC/c-Kit was quantified by densitometric analysis ($n = 4$). (**g**) Transmission electron micrographs of pMCs in $Pla2g3^{+/+}$ (+/+) and $Pla2g3^{-/-}$ (−/−) mice before (IgE-Ag (−)) and 2 min after (IgE-Ag (+)) stimulation with antigen. Scale bars, 2 μm. (**h**,**i**) Quantification of histamine content (**h**) and IgE-Ag–induced histamine release (quantity and percentage; **i**) in $Pla2g3^{+/+}$ (+/+) and $Pla2g3^{-/-}$ (−/−) pMCs. PEC, peritoneal cells. (**j**,**k**) Expression of mast-cell marker mRNAs (**j**) and dye extravasation in IgE-Ag–dependent PCA (**k**) in ears of $Pla2g3^{+/+}$ (+/+) or $Pla2g3^{-/-}$ (−/−) BMMC-reconstituted or nonreconstituted $Kit^{W\text{-}sh/W\text{-}sh}$ (W^{sh}) mice and wild-type (WT) $Kit^{+/+}$ mice. Data are compiled from two (**d**,**h**,**i**) or three (**b**,**c**,**e**,**j**,**k**) experiments (mean ± s.e.m., $*P < 0.05$; $**P < 0.01$). Images are representative of one (**f**) or two (**a**,**g**) experiments.

immaturity of mast cells (**Fig. 3a** and **Supplementary Fig. 2a**). After challenge with antigen, $Pla2g3^{+/+}$ skin mast cells exhibited features typical of degranulation, whereas $Pla2g3^{-/-}$ mast cells were almost insensitive. In agreement, the amount of histamine (**Fig. 3b**) and the expression of *Hdc* (which encodes histidine decarboxylase, a histamine-biosynthetic enzyme; **Fig. 3c**) were lower in the ears of $Pla2g3^{-/-}$ mice than in those of $Pla2g3^{+/+}$ mice. Enzymatic activity (**Fig. 3d**) and expression (**Fig. 3e**) of mast cell proteases, including chymase (encoded by *Mcpt4*), tryptase (encoded by *Mcpt6*) and carboxypeptidase (encoded by *Cpa3*), were also notably lower in the ears of $Pla2g3^{-/-}$ mice relative to $Pla2g3^{+/+}$ mice. However, expression of *Kit*, *Mitf* (which encodes a transcription factor essential for mast cell differentiation) and *Srgn* (which encodes serglycin, a proteoglycan core protein) was unchanged in ears of $Pla2g3^{-/-}$ mice (**Fig. 3e**), indicating that not all mast cell markers were affected by PLA2G3 deficiency. We confirmed the lower expression of HDC and the unaltered expression of c-Kit in the skin of $Pla2g3^{-/-}$ mice by immunoblotting (**Fig. 3f**).

$Pla2g3^{-/-}$ pMCs also had smaller and more irregular granules (**Fig. 3g** and **Supplementary Fig. 2b**), contained less histamine (**Fig. 3h**) and exhibited less IgE-Ag–induced histamine release (both amount and percentage; **Fig. 3i**) than $Pla2g3^{+/+}$ pMCs. Although the proportion of $Kit^{+}Fc\varepsilon RI\alpha^{+}$ skin mast cells or pMCs was similar in both genotypes, surface expression of FcεRIα was lower in $Pla2g3^{-/-}$ mice than in $Pla2g3^{+/+}$ mice (**Supplementary Fig. 2c**,**d**). A23187-induced histamine release by $Pla2g3^{-/-}$ pMCs was lower in terms of amount, but not percentage, compared to that by $Pla2g3^{+/+}$ pMCs (**Supplementary Fig. 2e**), suggesting that the attenuated IgE-Ag–induced degranulation and anaphylaxis in $Pla2g3^{-/-}$ mice was mainly due to the lower histamine content and surface FcεRI expression. Furthermore, intestinal expression of *Mcpt1* and *Mcpt2* (which encode mucosal mast-cell proteases) was markedly

lower in *Pla2g3*$^{-/-}$ mice than in *Pla2g3*$^{+/+}$ mice (**Supplementary Fig. 2f**). Thus, the lower anaphylaxis in *Pla2g3*$^{-/-}$ mice may result from abnormalities in the maturation and degranulation of mast cells in multiple anatomical sites. Other immune-cell populations in the skin and spleen were unaffected by PLA2G3 deficiency (**Supplementary Fig. 2g,h**).

To assess whether the aberrant features of mast cells in *Pla2g3*$^{-/-}$ mice relied on the absence of PLA2G3 in the mast cells themselves or in mast cell microenvironment, we transferred *Pla2g3*$^{+/+}$ or *Pla2g3*$^{-/-}$ BMMCs intradermally into mast cell–deficient *Kit*$^{W\text{-}sh/W\text{-}sh}$ mice. After 6 weeks, the distribution of mast cells in the ear dermis was comparable between mice reconstituted with *Pla2g3*$^{+/+}$ BMMCs and those reconstituted with *Pla2g3*$^{-/-}$ BMMCs (**Supplementary Fig. 3a**). Expression of mast-cell marker genes *Hdc*, *Mcpt4*, *Mcpt6* and *Cpa3* (**Fig. 3j**) and IgE-Ag–mediated PCA (**Fig. 3k** and **Supplementary Fig. 3b**) was much greater in the ears of mice that received *Pla2g3*$^{+/+}$ BMMCs over control *Kit*$^{W\text{-}sh/W\text{-}sh}$ mice, whereas these changes were scarcely seen in mice that received *Pla2g3*$^{-/-}$ BMMCs. We observed similar results when we transferred *Pla2g3*$^{+/+}$ or *Pla2g3*$^{-/-}$ BMMCs intravenously into *Kit*$^{W\text{-}sh/W\text{-}sh}$ mice. After 12 weeks of reconstitution, IgE-Ag–mediated PCA was restored in mice reconstituted with *Pla2g3*$^{+/+}$ BMMCs but remained poor in mice reconstituted with *Pla2g3*$^{-/-}$ BMMCs, although we observed similar numbers of reconstituted mast cells in the ear dermis (**Supplementary Fig. 3c,d**). In these experiments, low levels of mast-cell engraftment in the skin of *Kit*$^{W\text{-}sh/W\text{-}sh}$ mice relative to baseline amounts in the skin of wild-type mice restored PCA efficiently. *Kit*$^{W\text{-}sh/W\text{-}sh}$ mice transferred with *PLA2G3*$^{tg/+}$ BMMCs had a greater PCA response compared to those transferred with control BMMCs (**Supplementary Fig. 3e**). Altogether, the defective maturation and activation of mast cells in *Pla2g3*$^{-/-}$ mice are cell autonomous, even though the migration of mast cell progenitors into extravasuclar tissues is not profoundly impaired by PLA2G3 deficiency.

Impaired maturation of *Pla2g3*$^{-/-}$ mast cells in culture

Pla2g3$^{-/-}$ BMMCs grew normally in medium supplemented with IL-3 (**Supplementary Fig. 4a**) and, unlike tissue-resident mast cells, they had normal surface expression of FcεRIα (**Supplementary Fig. 4b**). Stimulation with IgE-Ag induced a robust release of $sPLA_2$ activity from wild-type BMMCs, whereas this release was ablated in *Pla2g3*$^{-/-}$ BMMCs and augmented in *PLA2G3*$^{tg/+}$ BMMCs (**Supplementary Fig. 4c,d**), confirming that PLA2G3 is released upon degranulation. IgE-Ag–stimulated *Pla2g3*$^{-/-}$ BMMCs released less histamine, PGD_2 and LTC_4 than *Pla2g3*$^{+/+}$ BMMCs, whereas these responses were greater in *PLA2G3*$^{tg/+}$ BMMCs than in control BMMCs (**Supplementary Fig. 4e–j**). IgE-Ag–induced influx of Ca^{2+}, induction of cytokines (encoded by *Il4*, *Il6* and *Tnf*) and phosphorylation of phospholipase C (PLCγ2) and Akt were similar between the genotypes (**Supplementary Fig. 4k–m**), suggesting that FcεRI-dependent signaling was not profoundly perturbed by PLA2G3 deficiency. Generation of eicosanoids by mast cells depends on $cPLA_2\alpha$, which is regulated by Ca^{2+}-dependent membrane translocation and MAP kinase-directed phosphorylation[17]. Consistent with the lower generation of eicosanoids (**Supplementary Fig. 4f,g**), FcεRI-dependent phosphorylation of ERK (not JNK and p38) and $cPLA_2\alpha$ and decrease in arachidonic acid–containing phosphatidylcholine were partially impaired in *Pla2g3*$^{-/-}$ BMMCs compared to *Pla2g3*$^{+/+}$ BMMCs, despite the equivalent expression of total ERK and $cPLA_2\alpha$ proteins in both cells (**Supplementary Fig. 4m–o**). Thus, PLA2G3 deficiency attenuates activation of ERK and $cPLA_2\alpha$ in BMMCs.

We took advantage of an *in vitro* system in which immature BMMCs undergo maturation toward mature CTMC-like cells in coculture with Swiss 3T3 fibroblasts[27]. PLA2G3 deficiency did not affect the proliferation of BMMCs in coculture (**Supplementary Fig. 5a**). During coculture, $sPLA_2$ activity was secreted from wild-type BMMCs in response to SCF, whereas $sPLA_2$ secretion was absent in *Pla2g3*$^{-/-}$ BMMCs and augmented in *PLA2G3*$^{tg/+}$ BMMCs (**Fig. 4a,b**). Although the ultrastructure of *Pla2g3*$^{-/-}$ BMMCs appeared normal, *Pla2g3*$^{-/-}$ CTMC-like cells contained unusual granules with less electron-dense contents than did *Pla2g3*$^{+/+}$ CTMC-like cells (**Fig. 4c** and **Supplementary Fig. 5b**). After coculture, the expression of *Hdc* (**Fig. 4d**) and its product histamine (**Fig. 4e**) were markedly greater in *Pla2g3*$^{+/+}$ CTMC-like cells, whereas these changes were barely seen in *Pla2g3*$^{-/-}$ cells. Even before coculture, *Hdc* expression and histamine content were slightly lower in *Pla2g3*$^{-/-}$ BMMCs than in *Pla2g3*$^{+/+}$ BMMCs, indicating that some early developmental process had already been perturbed by PLA2G3 deficiency. IgE-Ag–induced histamine release was greater in *Pla2g3*$^{+/+}$ cells after coculture than before coculture, whereas this coculture-driven increase in histamine release was impaired in *Pla2g3*$^{-/-}$ cells (**Fig. 4f**). Conversely, coculture-induced *Hdc* expression was greater in *PLA2G3*$^{tg/+}$ CTMC-like cells than in control cells (**Supplementary Fig. 5c**). Supplementation with PLA2G3 in coculture significantly restored the histamine level in *Pla2g3*$^{-/-}$ CTMC-like cells and also elevated it in *Pla2g3*$^{+/+}$ cells (**Fig. 4g**). *Pla2g3*$^{-/-}$ BMMCs without coculture did not respond to PLA2G3 (**Fig. 4g**), suggesting that the action of PLA2G3 on histamine synthesis in mast cells depends on fibroblasts. Histamine content in *Pla2g3*$^{+/+}$ BMMCs without coculture was substantially lower in the presence of PLA2G3 than its absence (**Fig. 4g**), which might reflect that the enzyme elicits the release of prestored histamine by degranulation (**Fig. 1b**).

The maturation of wild-type BMMCs to CTMC-like cells increased FcεRI-dependent PGD_2 synthesis (**Fig. 4h**), with a concomitant increase in *Ptgds2* (hematopoietic PGD_2 synthase; H-PGDS) (**Fig. 4i**). However, these changes in the PGD_2 pathway occurred only weakly in *Pla2g3*$^{-/-}$ cells. Surface expression of FcεRIα was significantly elevated in *Pla2g3*$^{+/+}$ cells but not in *Pla2g3*$^{-/-}$ cells after coculture (**Supplementary Fig. 5d**), consistent with the lower surface FcεRIα expression on tissue-resident mast cells in *Pla2g3*$^{-/-}$ mice. The coculture-driven induction of *Mcpt4* and *Mcpt6* (which encode mast cell proteases) and *Ndrg1* (which encodes a mast cell granule–associated protein[27]) was also impaired in *Pla2g3*$^{-/-}$ cells, whereas the constitutive expression of *Srgn* and *Kit* was unaffected (**Supplementary Fig. 5e**). We verified the attenuated induction of HDC and H-PGDS and the unaltered expression of c-Kit in *Pla2g3*$^{-/-}$ CTMC-like cells at the protein level (**Fig. 4j**). Although *Pla2g3*$^{+/+}$ CTMC-like cells acquired sensitivity to C48/80 after coculture[27], C48/80-induced degranulation (**Fig. 4k**) and induction of the putative C48/80 receptors encoded by *Mrgprx1* and *Mrgprx2* (ref. 28; **Supplementary Fig. 5e**) after coculture were lower in *Pla2g3*$^{-/-}$ cells. The coculture-dependent decrease in *Itga5* (which encodes integrin α_E) and increase in *Icam1* (which encodes integrin β_7), which participates in tissue homing of mast-cell progenitors[6], were unaffected by PLA2G3 deficiency (**Supplementary Fig. 5e**), consistent with the unaltered number of mast cells in *Pla2g3*$^{-/-}$ tissues. Microarray gene profiling using *Pla2g3*$^{+/+}$ and *Pla2g3*$^{-/-}$ BMMCs before and after coculture revealed that, of the ~41,000 genes examined, *Pla2g3*$^{+/+}$ cells expressed 3,632 coculture-inducible genes, of which 1,409 genes were barely or only partially induced in *Pla2g3*$^{-/-}$ cells. Genes affected by *Pla2g3* ablation included, for example, genes associated with secretory granules, genes related to biosynthesis or receptors for lipid mediators,

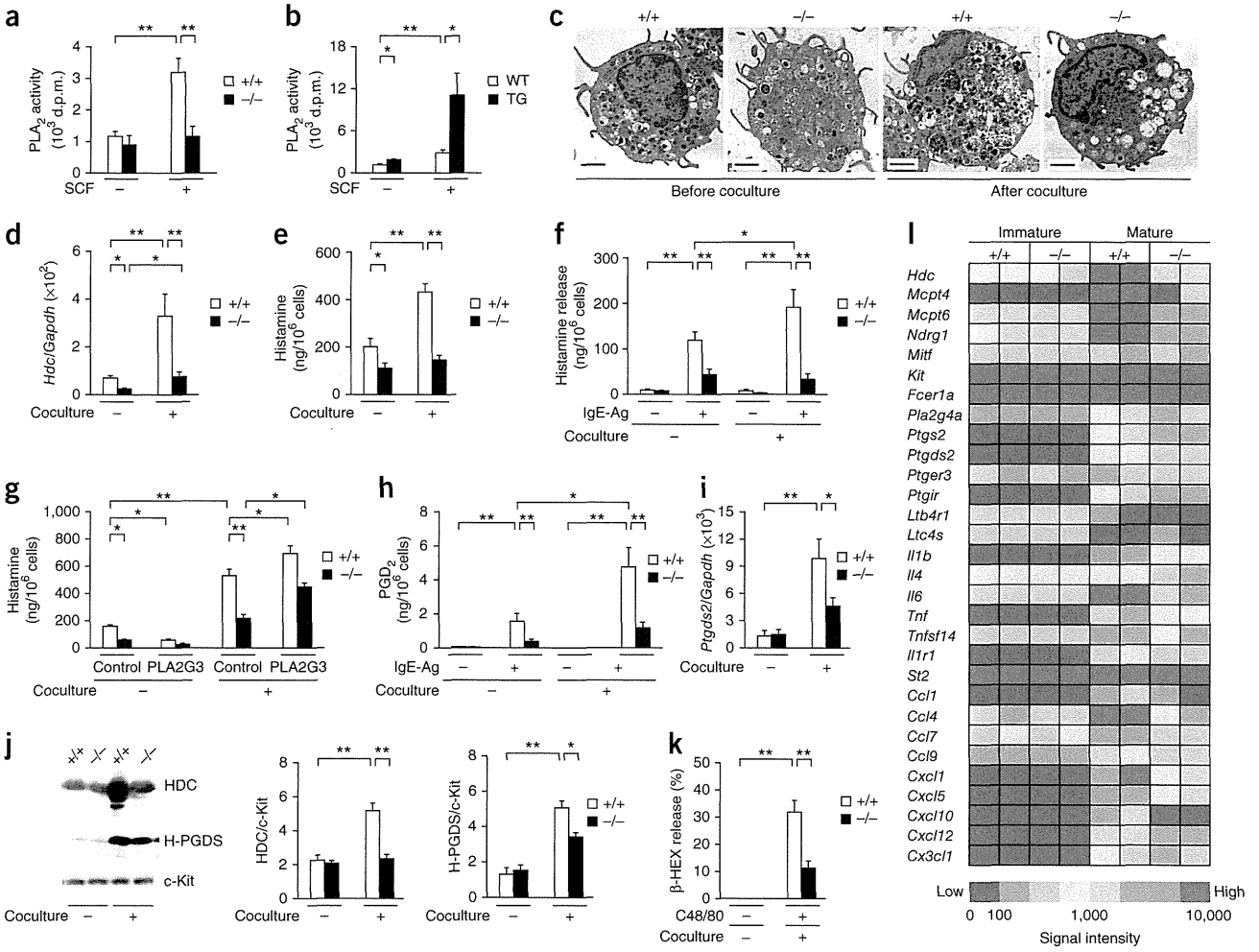

Figure 4 Defective fibroblast-driven maturation of *Pla2g3*$^{-/-}$ BMMCs. (**a**,**b**) Release of sPLA$_2$ activity from *Pla2g3*$^{+/+}$ (+/+) and *Pla2g3*$^{-/-}$ (−/−) BMMCs (**a**) or from *PLA2G3*$^{tg/+}$ (TG) and wild-type (WT) BMMCs (**b**) with or without 100 ng/ml SCF for 30 min ($n = 4$). d.p.m., disintegrations per minute. (**c**) Transmission electron microscopy of *Pla2g3*$^{+/+}$ (+/+) and *Pla2g3*$^{-/-}$ (−/−) BMMCs before and on day 4 of coculture with Swiss 3T3 fibroblasts. Scale bars, 2 μm. (**d**–**k**) Expression of *Hdc* relative to *Gapdh* ($n = 8$; **d**), cellular histamine levels ($n = 8$; **e**), histamine release with (IgE-Ag (+)) or without (IgE-Ag (−)) antigen challenge ($n = 8$; **f**), cellular histamine levels after culture in the presence or absence (control) of 2 μg/ml human PLA2G3 ($n = 6$; **g**), PGD_2 generation with or without antigen challenge ($n = 8$; **h**), *Ptgds2* expression ($n = 8$; **i**), immunoblot of HDC ($n = 6$) and H-PGDS ($n = 3$) relative to c-Kit (**j**) and C48/80-induced β-HEX release ($n = 7$; **k**) in *Pla2g3*$^{+/+}$ (+/+) or *Pla2g3*$^{-/-}$ (−/−) BMMCs before (−) and on day 4 of (+) coculture. (**l**) Microarray gene profile of *Pla2g3*$^{+/+}$ (+/+) and *Pla2g3*$^{-/-}$ (−/−) BMMCs before immature and on day 4 of mature coculture. Results from duplicate experiments are shown (columns). Heat maps are globally normalized for all genes. Data are from one experiment (**a**,**b**,**l**) and compiled from two (**d**,**e**,**g**,**j**,**k**) or three (**f**,**h**,**i**) experiments (mean ± s.e.m., $*P < 0.05$; $**P < 0.01$). Images in **c** are representative of two experiments.

and genes for cytokines, chemokines and their receptors (**Fig. 4l** and **Supplementary Table 1**), underscoring the immaturity of *Pla2g3*$^{-/-}$ cells, particularly after coculture.

By comparison, *Pla2g4a*$^{-/-}$ mice exhibited normal IgE-Ag–induced PCA, with normal counts of dermal mast cells and normal amounts of histamine (**Supplementary Fig. 5f–h**). IgE-Ag–induced histamine release, cellular histamine content and *Hdc* expression were unaffected by ablation of cPLA$_2$α (**Supplementary Fig. 5i–k**). Neither PGD_2 nor LTC_4 was produced by *Pla2g4a*$^{-/-}$ BMMCs (**Supplementary Fig. 5l,m**), confirming the obligatory role of cPLA$_2$α in eicosanoid synthesis in mast cells[29]. Thus, the absence of mast cell–derived eicosanoids by cPLA$_2$α deficiency did not affect maturation, degranulation and anaphylaxis of mast cells, suggesting that the effect of PLA2G3 deficiency on mast cells could not be simply explained by defective synthesis of eicosanoids by mast cells.

PGD_2-DP1 signals mast-cell maturation downstream of PLA2G3

To identify the specific lipid-mediator pathway that lies downstream of PLA2G3, we induced IgE-Ag–dependent PCA on mouse lines deficient in various eicosanoid receptors or biosynthetic enzymes. Of the eicosanoid receptor–deficient mouse lines tested, PCA was lower only in mice lacking the PGD receptor DP1 (*Ptgdr*$^{-/-}$)[9]. Vascular leakage was lower and ear mast cells exhibited poor degranulation despite an unaltered total count in *Ptgdr*$^{-/-}$ mice compared to wild-type mice (**Fig. 5a,b**). Dermal mast cells in *Ptgdr*$^{-/-}$ mice had fewer mature secretory granules, contained less histamine and were less sensitive to IgE-Ag–induced degranulation than those in *Ptgdr*$^{+/+}$ mice (**Fig. 5c,d**). Whereas the PCA was efficiently restored in *Kit*$^{W\text{-}sh/W\text{-}sh}$ mice reconstituted with *Ptgdr*$^{+/+}$ BMMCs, it was restored only partially in those mice reconstituted with *Ptgdr*$^{-/-}$ BMMCs (**Fig. 5e**). The PCA was unaltered or only slightly augmented in mice lacking other

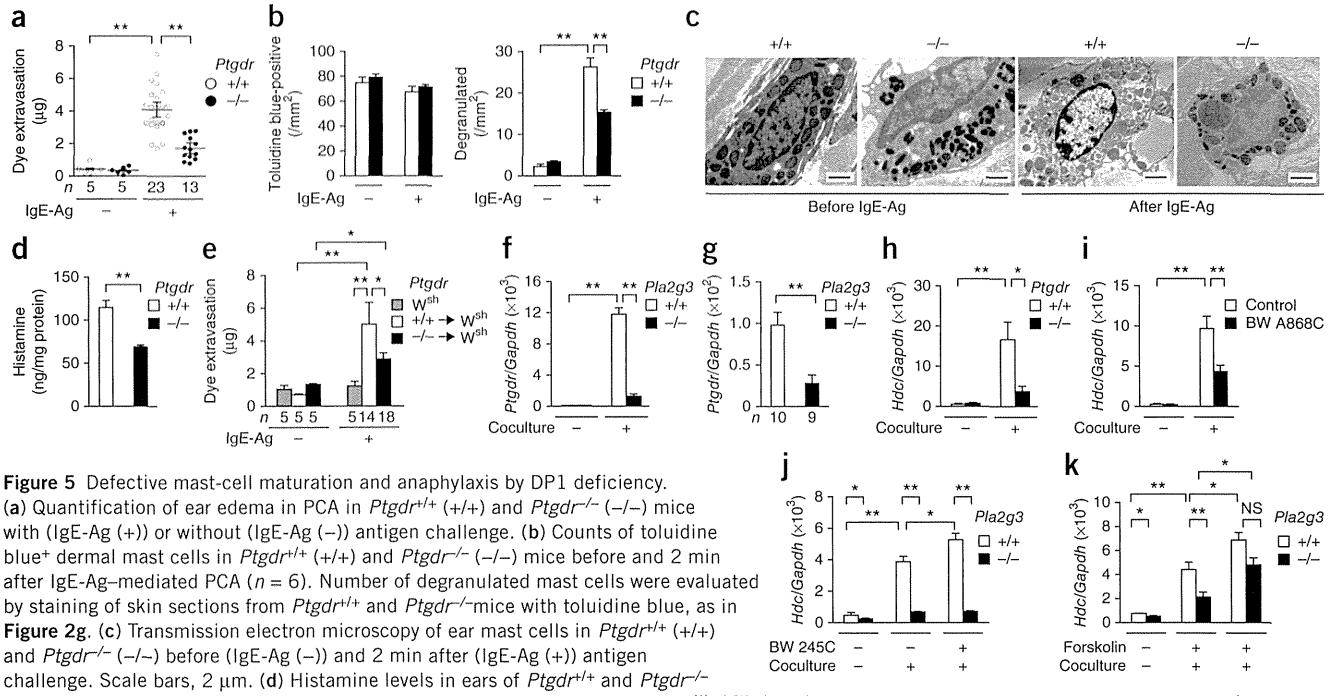

Figure 5 Defective mast-cell maturation and anaphylaxis by DP1 deficiency. (**a**) Quantification of ear edema in PCA in *Ptgdr*$^{+/+}$ (+/+) and *Ptgdr*$^{-/-}$ (−/−) mice with (IgE-Ag (+)) or without (IgE-Ag (−)) antigen challenge. (**b**) Counts of toluidine blue^{+} dermal mast cells in *Ptgdr*$^{+/+}$ (+/+) and *Ptgdr*$^{-/-}$ (−/−) mice before and 2 min after IgE-Ag–mediated PCA ($n = 6$). Number of degranulated mast cells were evaluated by staining of skin sections from *Ptgdr*$^{+/+}$ and *Ptgdr*$^{-/-}$mice with toluidine blue, as in **Figure 2g**. (**c**) Transmission electron microscopy of ear mast cells in *Ptgdr*$^{+/+}$ (+/+) and *Ptgdr*$^{-/-}$ (−/−) before (IgE-Ag (−)) and 2 min after (IgE-Ag (+)) antigen challenge. Scale bars, 2 μm. (**d**) Histamine levels in ears of *Ptgdr*$^{+/+}$ and *Ptgdr*$^{-/-}$ mice ($n = 10$). (**e**) Quantification of ear edema in IgE-Ag–dependent PCA in *Kit*$^{W\text{-}sh/W\text{-}sh}$ (W^{sh}) mice with or without reconstitution with *Ptgdr*$^{+/+}$ (+/+) or *Ptgdr*$^{-/-}$ (−/−) BMMCs. (**f**,**g**) Expression of *Ptgdr* in *Pla2g3*$^{+/+}$ and *Pla2g3*$^{-/-}$ BMMCs before and on day 2 of coculture ($n = 6$; **f**) and in the ear of *Pla2g3*$^{+/+}$ and *Pla2g3*$^{-/-}$ mice (**g**). (**h**,**i**) Expression of *Hdc* relative to *Gapdh* in *Ptgdr*$^{+/+}$ and *Ptgdr*$^{-/-}$ BMMCs ($n = 6$; **h**) or in wild-type BMMCs with or without BW A868C ($n = 7$; **i**) before and on day 2 of coculture. (**j**,**k**) Expression of *Hdc* relative to *Gapdh* in *Pla2g3*$^{+/+}$ and *Pla2g3*$^{-/-}$ BMMCs before and on day 2 of coculture with or without BW 245C ($n = 6$; **j**) or forskolin ($n = 6$; **k**). Data are compiled from two (**b**,**d**,**f**–**k**) or three (**a**,**e**) experiments (mean ± s.e.m., $^{*}P < 0.05$; $^{**}P < 0.01$; NS, not significant). Images in **c** are representative of two experiments.

eicosanoid receptors or biosynthetic enzymes (*Ptgdr2*$^{-/-}$, *Ptger1*$^{-/-}$, *Ptger2*$^{-/-}$, *Ptger3*$^{-/-}$, *Ptger4*$^{-/-}$, *Ptgfr*$^{-/-}$, *Ptgir*$^{-/-}$, *Tbxa2r*$^{-/-}$, *Ltb4r1*$^{-/-}$, *Ltb4r2*$^{-/-}$, *Ptges*$^{-/-}$, *Ptges2*$^{-/-}$ and *Alox15*$^{-/-}$; **Supplementary Fig. 6a**). Although *Ltc4s*$^{-/-}$ mice exhibited a lower PCA response as reported[10], their ear histamine content was unaffected (data not shown). Thus, abnormalities in mast cells observed in mice lacking PLA2G3 were phenocopied only in mice lacking DP1.

Next we examined the expression and function of DP1 in a mast cell–fibroblast coculture system[27]. Although we barely detected *Ptgdr* mRNA in BMMCs and Swiss 3T3 fibroblasts, *Ptgdr* mRNA was robustly induced in *Pla2g3*$^{+/+}$, but not in *Pla2g3*$^{-/-}$, CTMC-like cells after coculture (**Fig. 5f**). Consistently, *Ptgdr* expression in the ear was lower in *Pla2g3*$^{-/-}$ mice than in *Pla2g3*$^{+/+}$ mice (**Fig. 5g**). In agreement with the lower histamine amount in *Ptgdr*$^{-/-}$ dermal mast cells (**Fig. 5d**), the coculture-driven *Hdc* induction was severely impaired in *Ptgdr*$^{-/-}$ CTMC-like cells (**Fig. 5h**). In addition, the DP1 antagonist BW A868C prevented the coculture-induced upregulation of *Hdc* in wild-type CTMC-like cells (**Fig. 5i**). Conversely, the DP1 agonist BW 245C significantly enhanced *Hdc* induction in wild-type CTMC-like cells (**Fig. 5j**). However, the coculture-driven *Hdc* expression was barely restored by BW 245C in *Pla2g3*$^{-/-}$ mice (**Fig. 5j**), likely because DP1 induction was blunted by PLA2G3 deficiency (**Fig. 5f**). To circumvent this problem, we used the cAMP-elevating agent forskolin because DP1 is coupled with Gs-cAMP signaling[9]. The addition of forskolin to the coculture bypassed the requirement for DP1 in the induction of *Hdc* in *Pla2g3*$^{-/-}$ CTMC-like cells (**Fig. 5k**). By comparison, the expression of *Ptgdr2*, which encodes another PGD_2 receptor known as CRTH2, was high in BMMCs and lowered in accordance with their maturation into CTMC-like cells, without being affected by the *Pla2g3* genotypes (**Supplementary Fig. 6b**). Moreover, *Hdc* induction in CTMC-like cells was unaffected by CRTH2 deficiency in coculture, and *Ptgdr2* expression was unaffected by PLA2G3 deficiency *in vivo* (**Supplementary Fig. 6c**,**d**). The coculture-driven production of other eicosanoids such as 15-HETE and PGI_2 was unaffected by PLA2G3 deficiency (**Supplementary Fig. 6e**). Thus, DP1-cAMP signaling is specifically required for the PLA2G3-dependent maturation of mast cells.

L-PGDS supplies a PGD_2 pool for mast-cell maturation

We hypothesized that the absence of PGD_2 biosynthetic enzyme(s), acting downstream of PLA2G3 and upstream of DP1, would also influence maturation of mast cells. Of the two PGD_2 synthase–encoding genes, *Ptgds2* (which encodes H-PGDS) was expressed in BMMCs but not in Swiss 3T3 fibroblasts, whereas *Ptgds* (which encodes lipocalin-type PGDS; L-PGDS) expression was higher in fibroblasts than in BMMCs (**Fig. 6a**) and was below the detection limit in pMCs (data not shown). L-PGDS immunoreactivity was associated with fibroblasts surrounding toluidine blue^{+} mast cells in mouse skin (**Supplementary Fig. 7a**). PCA was exacerbated in *Ptgds2*$^{-/-}$ mice[30], which lack H-PGDS (**Fig. 6b**), whereas it was suppressed in *Ptgds*$^{-/-}$ mice[31], which lack L-PGDS (**Fig. 6c**), in comparison with respective control mice. *Ptgds*$^{-/-}$ mice had fewer degranulated ear mast cells than did *Ptgds*$^{+/+}$ mice after antigen challenge, although the total mast cell count was unaffected (**Fig. 6d**). Dermal mast cells in *Ptgds*$^{-/-}$ mice were ultrastructurally immature (that is, cytoplasmic granules were small and heterogeneous), comparatively resistant to antigen-induced degranulation, and contained less histamine than those in *Ptgds*$^{+/+}$ mice (**Fig. 6e**,**f**). Thus, the notable similarity among *Pla2g3*$^{-/-}$, *Ptgds*$^{-/-}$ and *Ptgdr*$^{-/-}$ mice suggests that PLA2G3, L-PGDS and DP1 may lie in the same

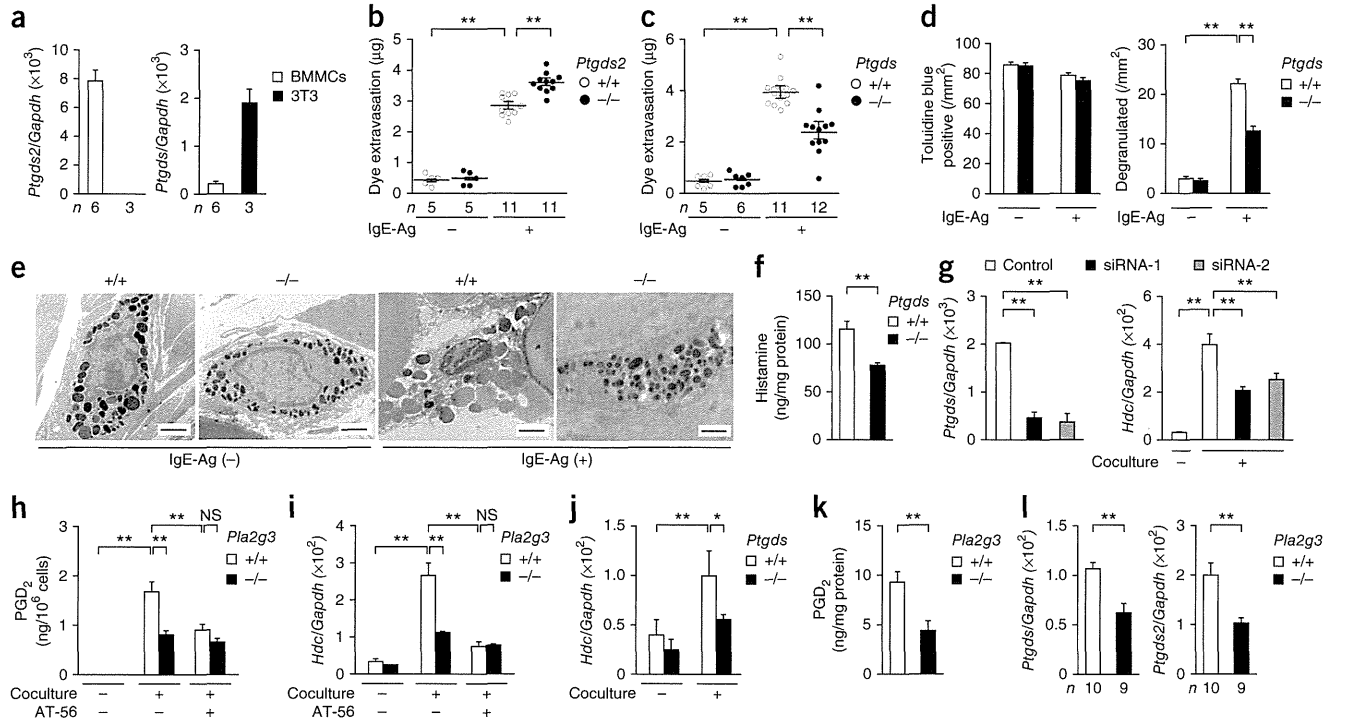

Figure 6 Defective mast-cell maturation and anaphylaxis by L-PGDS deficiency. (**a**) Expression of *Ptgds* and *Ptgds2* relative to *Gapdh* in wild-type BMMCs and Swiss 3T3 fibroblasts. (**b**,**c**) Quantification of ear edema in PCA in *Ptgds*$^{-/-}$ (**b**), *Ptgds2*$^{-/-}$ (**c**) mice (−/−) and littermate wild-type (+/+) mice with (IgE-Ag (+)) or without (IgE-Ag (−)) antigen challenge. (**d**) Dermal mast-cell counts in *Ptgds*$^{+/+}$ and *Ptgds*$^{-/-}$ mice before and 2 min after IgE-Ag–mediated PCA ($n = 6$). Number of degranulated mast cells were evaluated by staining of skin sections with toluidine blue, as in **Figure 2g**. (**e**) Transmission electron microscopy of *Ptgds*$^{+/+}$ (+/+) and *Ptgds*$^{-/-}$ (−/−) ear mast cells before (IgE-Ag (−)) and 2 min after (IgE-Ag (+)) antigen challenge. Scale bars, 2 μm. (**f**) Histamine levels in ears of *Ptgds*$^{+/+}$ and *Ptgds*$^{-/-}$ mice ($n = 10$). (**g**) *Ptgds* expression in Swiss 3T3 fibroblasts after *Ptgds* or scrambled siRNA treatment and *Hdc* expression in wild-type BMMCs before and on day 2 of coculture with siRNA-treated fibroblasts ($n = 7$). (**h**,**i**) PGD_2 generation (**h**) and *Hdc* expression (**i**) before and on day 1 of coculture of *Pla2g3*$^{+/+}$ or *Pla2g3*$^{-/-}$ BMMCs with Swiss 3T3 fibroblasts with or without AT-56 ($n = 6$). (**j**) *Hdc* expression in wild-type BMMCs before and on day 4 of coculture with *Ptgds*$^{+/+}$ (+/+) or *Ptgds*$^{-/-}$ (−/−) skin fibroblasts ($n = 6$). (**k**,**l**) PGD_2 levels ($n = 10$; **k**) and *Ptgds* and *Ptgds2* expression (**l**) in the ear skin of *Pla2g3*$^{+/+}$ and *Pla2g3*$^{-/-}$ mice. Data are compiled from two (**a**,**d**,**f**,**h**–**l**) or three (**b**,**c**,**g**) experiments (mean ± s.e.m., $*P < 0.05$; $**P < 0.01$; NS, not significant). Images in **e** are representative of two experiments.

regulatory pathway driving maturation of mast cells. The transfer of *Ptgds*$^{+/+}$ or *Ptgds*$^{-/-}$ BMMCs into *Kit*$^{W\text{-}sh/W\text{-}sh}$ mice fully restored the PCA response (**Supplementary Fig. 7b**), and a similar induction of *Hdc* occurred when *Ptgds*$^{+/+}$ or *Ptgds*$^{-/-}$ BMMCs were cultured with fibroblasts (**Supplementary Fig. 7c**), indicating that L-PGDS in fibroblasts, not in mast cells, may be important for the regulation of mast cells.

Coculture with L-PGDS–silenced Swiss 3T3 fibroblasts by two distinct *Ptgds*-specific small interfering (si)RNAs resulted in less induction of *Hdc* in wild-type CTMC-like cells (**Fig. 6g**). PGD_2 generation after coculture of parent fibroblasts with *Pla2g3*$^{-/-}$ BMMCs was ~50% lower than with *Pla2g3*$^{+/+}$ BMMCs (**Fig. 6h**). The L-PGDS inhibitor AT-56 lowered PGD_2 generation and *Hdc* induction in *Pla2g3*$^{+/+}$ cocultures to amounts similar to those in *Pla2g3*$^{-/-}$ cocultures, although it did not affect these responses in *Pla2g3*$^{-/-}$ cocultures (**Fig. 6h,i** and **Supplementary Fig. 7d**). *Hdc* induction in wild-type BMMCs also occurred in coculture with primary skin fibroblasts from *Ptgds*$^{+/+}$ mice, whereas this response was impaired in coculture with those from *Ptgds*$^{-/-}$ mice (**Fig. 6j**). Thus, the augmentative effects of PLA2G3 on coculture-driven synthesis of PGD_2 and histamine were abrogated when L-PGDS in fibroblasts was ablated. L-PGDS–dependent production of PGD_2, as revealed by coculture of *Ptgds2*$^{-/-}$ BMMCs with Swiss 3T3 fibroblasts, occurred gradually over a long period, whereas H-PGDS–dependent production of PGD_2 was transient, albeit robust (**Supplementary Fig. 7e**), suggesting that the continuous supply of PGD_2 by L-PGDS is crucial for maturation of mast cells.

Additionally, we observed robust upregulation of *Ptgds2* in BMMCs and *Ptgds* in Swiss 3T3 fibroblasts or in primary mouse skin fibroblasts (and to a much lesser extent in BMMCs) in wild-type BMMC cocultures, whereas these responses occurred only partially in *Pla2g3*$^{-/-}$ BMMC cocultures (**Supplementary Fig. 7f–h**). Conversely, induction of *Ptgds* in Swiss 3T3 fibroblasts was enhanced in coculture with *PLA2G3*$^{tg/+}$ BMMCs relative to wild-type BMMCs (**Supplementary Fig. 7i**). Thus, not only did mast cell–derived PLA2G3 supply arachidonic acid to L-PGDS in fibroblasts, it also contributed to induced expression of L-PGDS for efficient biosynthesis of a pool of PGD_2 that promotes maturation of mast cells. However, addition of PLA2G3 or BV-PLA_2 alone did not increase *Ptgds* expression in fibroblasts (**Supplementary Fig. 7j**), suggesting that some additional mast cell–derived factor(s) may be required for the induction of L-PGDS in fibroblasts. In agreement with the *in vitro* studies, amounts of PGD_2 (**Fig. 6k**) and expression of two PGDSs (**Fig. 6l**) were significantly lower in the ear of *Pla2g3*$^{-/-}$ mice than that of *Pla2g3*$^{+/+}$ mice, confirming the coupling of PLA2G3 with PGD_2 synthesis *in vivo*. Thus, PLA2G3 secreted from mast cells is

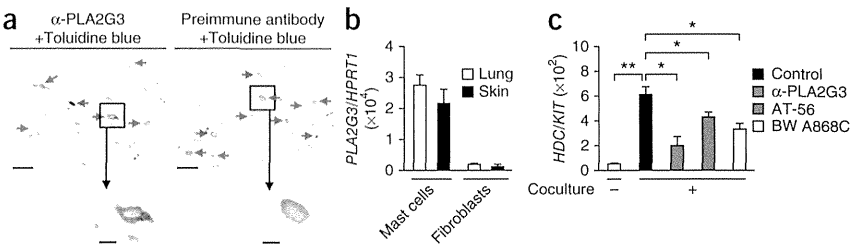

Figure 7 The PLA2G3–L-PGDS–DP1 axis facilitates maturation of human mast cells. (**a**) Immunohistochemistry analysis of human skin sections (atopic dermatitis) with anti-PLA2G3 (α-PLA2G3) or a preimmune antibody, followed by counterstaining with toluidine blue (scale bars, 50 μm). Blue and red arrows indicate resting and degranulated mast cells, respectively. Boxed areas are magnified below (scale bars, 5 μm). (**b**) Expression of *PLA2G3* relative to *HRPT1* in primary mast cells and fibroblasts obtained from human skin and lung ($n = 3$). (**c**) Expression of *HDC* relative to *KIT* in human lung mast cells before or on day 4 of coculture with human lung fibroblasts in the presence or absence of 5 μg/ml anti-PLA2G3, 10 μM AT-56 or 1 μM BW A868C ($n = 4$). Data are from one experiment (**b**,**c**; mean ± s.e.m., $*P < 0.05$; $**P < 0.01$). Images in **a** are representative of two experiments.

linked to fibroblastic L-PGDS–dependent synthesis of PGD_2, which in turn activates DP1 induced on mast cells to assist their terminal maturation toward a fully anaphylaxis-sensitive CTMC-like phenotype (**Supplementary Fig. 7k**).

PLA2G3 PGD_2 axis induces maturation of human mast cells

In human skin, toluidine blue$^+$ dermal mast cells showed PLA2G3 immunoreactivity, although some toluidine blue$^-$ cells also appeared PLA2G3$^+$ (**Fig. 7a**). We detected *PLA2G3* mRNA expression in mast cells in preference to fibroblasts obtained from human lung and skin (**Fig. 7b**). *HDC* mRNA expression was robustly induced in human lung mast cells after coculture with human lung fibroblasts, and this induction was suppressed either by anti-PLA2G3, by L-PGDS inhibitor (AT-56) or by DP1 antagonist (BW A868C) to a similar extent (**Fig. 7c**). Thus, the fibroblast-dependent *HDC* induction in human mast cells also depends on the PLA2G3–L-PGDS–DP1 pathway.

DISCUSSION

Here we showed that PLA2G3, a major $sPLA_2$ in mast cells, contributed to anaphylaxis by inducing maturation of mast cells in concert with adjacent fibroblasts through a unique pathway involving a cell-to-cell loop of the biosynthetic and receptor pathway for PGD_2. Promotion of mast cell maturation by PGD_2-DP1 signaling provides a mechanistic explanation for the protective effect of systemic DP1 ablation on asthma[9]. The paracrine PGD_2 circuit driven by PLA2G3, an 'anaphylactic $sPLA_2$', is a previously unidentified lipid-orchestrated pathway linked to allergy and uncovers a missing microenvironmental cue underlying the proper maturation of mast cells.

The SCF–c-Kit system, in cooperation with transcription factors, integrins or accessory cytokines, is essential for the development, homing, proliferation and differentiation of mast cells[3–7]. However, SCF alone is insufficient to drive the full maturation of mast cells, leading to the hypothesis that some other stromal factor(s) may be additionally required. These signals may include, for instance, interleukin 33, nerve growth factor, the morphogen TGF-β, hyaluronic acid and the adhesion molecule SgIGSF (spermatogenic immunoglobulin superfamily)[3,4,7], although their *in vivo* relevancies have not yet been fully understood. As in mice lacking PLA2G3, mast cells in mice lacking histamine (*Hdc*$^{-/-}$) or heparin (*Ndst2*$^{-/-}$ or *Srgn*$^{-/-}$) are immature and have low histamine content[32–34], suggesting that the lower amount of histamine may underlie, at least in part, the defective maturation of mast cells. We showed here that a signal driven by PGD_2, a bioactive lipid, is a missing link required for the fibroblast-driven maturation of mast cells. The PLA2G3–L-PGDS–DP1 circuit revealed the paracrine action of $sPLA_2$ in the biosynthetic mobilization of PGD_2 by proximal cells, the functional segregation of the two PGDS enzymes in distinct cell populations and a new aspect of PGD_2-DP1 signaling in promoting maturation of mast cells and thereby allergy. Moreover, our results revealed a previously unidentified aspect of the stromal cytokine SCF, which triggers this unique lipid-driven pathway by inducing PLA2G3 secretion from mast cells.

L-PGDS, a fibroblast-cell enzyme, acts downstream of PLA2G3 to supply PGD_2 to DP1 in mast cells to drive their terminal maturation. Contrary to our prediction, PGD_2 driven by H-PGDS, a mast cell enzyme, had an anti-allergy role, a view that is consistent with the exacerbated allergen-induced contact dermatitis in *Ptgds2*$^{-/-}$ mice[11]. Although it is unclear how the L-PGDS–driven extrinsic, but not the H-PGDS–driven intrinsic, pool of PGD_2 is preferentially used by DP1 on mast cells, we speculate that the prolonged supply of PGD_2 by L-PGDS, rather than its transient supply by H-PGDS, may be suitable for a long-lasting cell differentiation process. Alternatively, the PGD_2 captured by L-PGDS, a lipid carrier protein (lipocalin), may be stabilized or better presented to mast cell DP1. This idea is reminiscent of a finding that lysophosphatidic acid (LPA), another lipid mediator, is presented to its cognate receptor as a complex with autotaxin, an LPA-producing enzyme[35]. The spatiotemporal discrimination of distinct PGD_2 pools is also supported by the fact that although PGD_2 promotes Th2-based asthma[9], it contributes to resolution of inflammation through limiting neutrophil infiltration, dendritic cell activation or other mechanisms[11–13].

The paracrine PLA2G3–L-PGDS–DP1 circuit could not be compensated by other PLA_2 enzymes, implying a specific role of this atypical $sPLA_2$. We observed no defects in maturation of mast cells or anaphylaxis even in mice lacking $cPLA_2\alpha$, although mild developmental changes in *Pla2g4a*$^{-/-}$ BMMCs have been reported, probably because of different culture conditions[29]. Presumably, ablation of only the specific and local lipid mediator pathway by PLA2G3 deficiency, in contrast to ablation of bulk eicosanoids in both mast cells and microenvironments by $cPLA_2\alpha$ deficiency[29], may have a different impact on mast cells. The phenotypes observed in *Pla2g3*$^{-/-}$ mice tend to be more severe than those observed in *Ptgdr*$^{-/-}$ or *Ptgds*$^{-/-}$ mice, suggesting that PLA2G3 might be also coupled with other lipid signal(s) that could act in concert with the L-PGDS–DP1 axis to promote full maturation of mast cells. Such lipid candidates include LPA and lysophosphatidylserine, which can affect mast cell development and activation[36,37]. Not only can lysophospholipids transmit signals through their specific receptors, but they can also facilitate the opening of Ca^{2+} channels, which might explain the degranulation-promoting effect of PLA2G3 on mast cells.

Although it has been proposed that $sPLA_2$ enzymes, after being secreted, may act on neighboring cells or extracellular phospholipids to augment lipid mediator biosynthesis, this idea has yet to gain traction because *in vivo* evidence is largely lacking. Our study provides to our knowledge the first clear *in vivo* evidence that $sPLA_2$ acts in this

manner, thus providing a rationale for the long-standing question on the role of the secreted type of PLA_2. This extracellular PLA_2 family, through a paracrine process, regulates homeostasis and pathology in response to a given microenvironmental cue. Given that PLA2G3 is insensitive to classical $sPLA_2$ inhibitors, a new agent that specifically inhibits this unique $sPLA_2$ may be useful for the treatment of patients with mast cell–associated allergic and other diseases.

METHODS

Methods and any associated references are available in the online version of the paper.

Accession code. Gene Expression Ominibus: GSE44980 (microarray data).

Note: Supplementary information is available in the online version of the paper.

ACKNOWLEDGMENTS

We thank Y. Tanoue, H. Ohkubo, K. Araki and K. Yamamura for generating *Ptges2*$^{-/-}$ mice. This work was supported by grants-in-aid for Scientific Research from the Ministry of Education, Culture, Sports, Science and Technology of Japan (22116005 and 24390021 to M.M. and 23790119 and 24117724 to Y.T.), Promoting Individual Research to Nurture the Seeds of Future Innovation and Organizing Unique Innovative Network (PRESTO) of Japan Science and Technology Agency (to M.M.), and the Uehara, Mitsubishi, Terumo, Mochida and Toray Science Foundations (to M.M.).

AUTHOR CONTRIBUTIONS

Y.T. performed experiments and together with M.M. conceived and designed the study, interpreted the findings and wrote the manuscript; N.U., T.K., M.K., R.M. and H.S. performed experiments; S.T., M.S., Masanori Nakamura, Y.N., K.I., K.M., Satoshi Nakamizo, K.K., Y.O. and C.R. helped perform some experiments; K.Y., N.K., R.T., M.H.G. M.A., T.Y., Masataka Nakamura, K.W., H.H., Motonao Nakamura, K.A., Y.U., Y.S., T.S., Shu Narumiya and S.H. contributed to experimental designs.

COMPETING FINANCIAL INTERESTS

The authors declare no competing financial interests.

1. Galli, S.J. & Tsai, M. IgE and mast cells in allergic disease. *Nat. Med.* **18**, 693–704 (2012).
2. Gurish, M.F. & Austen, K.F. Developmental origin and functional specialization of mast cell subsets. *Immunity* **37**, 25–33 (2012).
3. Allakhverdi, Z., Smith, D.E., Comeau, M.R. & Delespesse, G. Cutting edge: The ST2 ligand IL-33 potently activates and drives maturation of human mast cells. *J. Immunol.* **179**, 2051–2054 (2007).
4. Matsuda, H. *et al.* Nerve growth factor induces development of connective tissue-type mast cells *in vitro* from murine bone marrow cells. *J. Exp. Med.* **174**, 7–14 (1991).
5. Abonia, J.P. *et al.* Constitutive homing of mast cell progenitors to the intestine depends on autologous expression of the chemokine receptor CXCR2. *Blood* **105**, 4308–4313 (2005).
6. Gurish, M.F. *et al.* Intestinal mast cell progenitors require CD49dβ7 (α4β7 integrin) for tissue-specific homing. *J. Exp. Med.* **194**, 1243–1252 (2001).
7. Ito, A. *et al.* SgIGSF: a new mast-cell adhesion molecule used for attachment to fibroblasts and transcriptionally regulated by MITF. *Blood* **101**, 2601–2608 (2003).
8. Shimizu, T. Lipid mediators in health and disease: enzymes and receptors as therapeutic targets for the regulation of immunity and inflammation. *Annu. Rev. Pharmacol. Toxicol.* **49**, 123–150 (2009).
9. Matsuoka, T. *et al.* Prostaglandin D_2 as a mediator of allergic asthma. *Science* **287**, 2013–2017 (2000).
10. Kanaoka, Y., Maekawa, A., Penrose, J.F., Austen, K.F. & Lam, B.K. Attenuated zymosan-induced peritoneal vascular permeability and IgE-dependent passive cutaneous anaphylaxis in mice lacking leukotriene C_4 synthase. *J. Biol. Chem.* **276**, 22608–22613 (2001).
11. Trivedi, S.G. *et al.* Essential role for hematopoietic prostaglandin D_2 synthase in the control of delayed type hypersensitivity. *Proc. Natl. Acad. Sci. USA* **103**, 5179–5184 (2006).
12. Hammad, H. *et al.* Activation of the D prostanoid 1 receptor suppresses asthma by modulation of lung dendritic cell function and induction of regulatory T cells. *J. Exp. Med.* **204**, 357–367 (2007).
13. Levy, B.D., Clish, C.B., Schmidt, B., Gronert, K. & Serhan, C.N. Lipid mediator class switching during acute inflammation: signals in resolution. *Nat. Immunol.* **2**, 612–619 (2001).
14. Kunikata, T. *et al.* Suppression of allergic inflammation by the prostaglandin E receptor subtype EP3. *Nat. Immunol.* **6**, 524–531 (2005).
15. Serhan, C.N., Chiang, N. & Van Dyke, T.E. Resolving inflammation: dual anti-inflammatory and pro-resolution lipid mediators. *Nat. Rev. Immunol.* **8**, 349–361 (2008).
16. Murakami, M. *et al.* Recent progress in phospholipase A_2 research: From cells to animals to humans. *Prog. Lipid Res.* **50**, 152–192 (2011).
17. Uozumi, N. *et al.* Role of cytosolic phospholipase A_2 in allergic response and parturition. *Nature* **390**, 618–622 (1997).
18. Munoz, N.M. *et al.* Deletion of secretory group V phospholipase A_2 attenuates cell migration and airway hyperresponsiveness in immunosensitized mice. *J. Immunol.* **179**, 4800–4807 (2007).
19. Henderson, W.R. Jr. *et al.* Importance of group X-secreted phospholipase A_2 in allergen-induced airway inflammation and remodeling in a mouse asthma model. *J. Exp. Med.* **204**, 865–877 (2007).
20. Bilo, B.M., Rueff, F., Mosbech, H., Bonifazi, F. & Oude-Elberink, J.N. Diagnosis of Hymenoptera venom allergy. *Allergy* **60**, 1339–1349 (2005).
21. Dudler, T. *et al.* A link between catalytic activity, IgE-independent mast cell activation, and allergenicity of bee venom phospholipase A_2. *J. Immunol.* **155**, 2605–2613 (1995).
22. Sato, H. *et al.* Group III secreted phospholipase A_2 regulates epididymal sperm maturation and fertility in mice. *J. Clin. Invest.* **120**, 1400–1414 (2010).
23. Murakami, M. *et al.* Cellular distribution, post-translational modification, and tumorigenic potential of human group III secreted phospholipase A_2. *J. Biol. Chem.* **280**, 24987–24998 (2005).
24. Murakami, M. *et al.* Cellular arachidonate-releasing function of novel classes of secretory phospholipase A_2s (groups III and XII). *J. Biol. Chem.* **278**, 10657–10667 (2003).
25. Valentin, E., Ghomashchi, F., Gelb, M.H., Lazdunski, M. & Lambeau, G. Novel human secreted phospholipase A_2 with homology to the group III bee venom enzyme. *J. Biol. Chem.* **275**, 7492–7496 (2000).
26. Sato, H. *et al.* Analyses of group III secreted phospholipase A_2 transgenic mice reveal potential participation of this enzyme in plasma lipoprotein modification, macrophage foam cell formation, and atherosclerosis. *J. Biol. Chem.* **283**, 33483–33497 (2008).
27. Taketomi, Y. *et al.* Impaired mast cell maturation and degranulation and attenuated allergic responses in *Ndrg1*-deficient mice. *J. Immunol.* **178**, 7042–7053 (2007).
28. Kashem, S.W. *et al.* G protein coupled receptor specificity for C3a and compound 48/80-induced degranulation in human mast cells: roles of Mas-related genes MrgX1 and MrgX2. *Eur. J. Pharmacol.* **668**, 299–304 (2011).
29. Nakatani, N. *et al.* Role of cytosolic phospholipase A_2 in the production of lipid mediators and histamine release in mouse bone-marrow-derived mast cells. *Biochem. J.* **352**, 311–317 (2000).
30. Mohri, I. *et al.* Prostaglandin D_2-mediated microglia/astrocyte interaction enhances astrogliosis and demyelination in twitcher. *J. Neurosci.* **26**, 4383–4393 (2006).
31. Eguchi, N. *et al.* Lack of tactile pain (allodynia) in lipocalin-type prostaglandin D synthase-deficient mice. *Proc. Natl. Acad. Sci. USA* **96**, 726–730 (1999).
32. Ohtsu, H. *et al.* Mice lacking histidine decarboxylase exhibit abnormal mast cells. *FEBS Lett.* **502**, 53–56 (2001).
33. Forsberg, E. *et al.* Abnormal mast cells in mice deficient in a heparin-synthesizing enzyme. *Nature* **400**, 773–776 (1999).
34. Humphries, D.E. *et al.* Heparin is essential for the storage of specific granule proteases in mast cells. *Nature* **400**, 769–772 (1999).
35. Nishimasu, H. *et al.* Crystal structure of autotaxin and insight into GPCR activation by lipid mediators. *Nat. Struct. Mol. Biol.* **18**, 205–212 (2011).
36. Bagga, S. *et al.* Lysophosphatidic acid accelerates the development of human mast cells. *Blood* **104**, 4080–4087 (2004).
37. Iwashita, M. *et al.* Synthesis and evaluation of lysophosphatidylserine analogues as inducers of mast cell degranulation. Potent activities of lysophosphatidylthreonine and its 2-deoxy derivative. *J. Med. Chem.* **52**, 5837–5863 (2009).

ONLINE METHODS

Mice. *Pla2g3*$^{-/-}$, *Pla2g4a*$^{-/-}$, *Pla2g5*$^{-/-}$, *Pla2g10*$^{-/-}$, *Ptgdr*$^{-/-}$, *Ptgdr2*$^{-/-}$, *Ptgds*$^{-/-}$, *Ptgds2*$^{-/-}$, *Ptges*$^{-/-}$, *Ptger1*$^{-/-}$, *Ptger2*$^{-/-}$, *Ptger3*$^{-/-}$, *Ptger4*$^{-/-}$, *Ptgfr*$^{-/-}$, *Ptgir*$^{-/-}$, *Tbxa2r*$^{-/-}$, *Ltb4r1*$^{-/-}$, *Ltb4r2*$^{-/-}$, *Ltc4s*$^{-/-}$, *Alox15*$^{-/-}$ and *PLA2G3*$^{tg/+}$ mice have been described previously[9,14,17–19,22,26,38–44]. *Ptges2*$^{-/-}$ mice (RIKEN RBRC04849) were generated by the Institute of Resource Development and Analysis (Kumamoto University). *Pla2g2d*$^{-/-}$, *Pla2g2e*$^{-/-}$ and *Pla2g2f*$^{-/-}$ mice were generated by the Transgenic Resources Program (Department of Comparative Medicine, University of Washington; unpublished data). These mice were backcrossed to C57BL/6 mice for more than 11 generations, except for *Pla2g3*$^{-/-}$ and *Ptger4*$^{-/-}$ mice (129Sv × C57BL/6), which were from the third backcrosses to C57BL/6 mice owing to severe problems in reproduction[22] and neonatal death[39], respectively, particularly after successive backcrossing onto the C57BL/6 background. All experiments using knockout or transgenic mice (male, 8–12-week-old) were compared with their age-matched littermate control mice. Mast cell–deficient *Kit* mutant mice, C57BL/6J-*Kit*$^{W-sh/W-sh}$ and WBB6F$_1$-*Kit*$^{W/W-v}$, were purchased from the Jackson Laboratories and Japan SLC, respectively. All mice were housed in climate-controlled (23 °C) specific pathogen–free facilities with a 12-h light-dark cycle, with free access to standard laboratory food (CE2; CLEA) and water. All animal experiments were performed in accordance with protocols approved by the Institutional Animal Care and Use Committees of the Tokyo Metropolitan Institute of Medical Science and Showa University, in accordance with the Standards Relating to the Care and Management of Experimental Animals in Japan.

PLA_2 assay. BV-PLA_2 was purchased from Sigma-Aldrich. Recombinant mature human PLA2G3 protein was expressed in silkworms by the baculovirus system and purified to near homogenity by an affinity column conjugated with mouse monoclonal anti–human PLA2G3 (5D2F1; IgG), as described previously[26]. PLA_2 activities in the supernatants of mast cells were assayed by measuring the amounts of [^{14}C]linoleic acid released from 1-palmitoyl-2-[^{14}C]linoleoyl-phosphatidylethanolamine (Perkin Elmer). Each reaction mixture consisted of appropriate amounts of the samples, 100 mM Tris-HCl (pH 7.4), 4 mM $CaCl_2$ and the substrate at 1 μM. After incubation for 2 h at 37 °C, [^{14}C]linoleic acid was extracted, and the radioactivity was quantified with a liquid scintillation counter (LS5801; Beckman), as described previously[22–24].

Anaphylaxis. For PSA, mice were intravenously injected with 3 μg of monoclonal anti-DNP IgE (SPE-7; Sigma-Aldrich). After 24 h, the mice were challenged intravenously with 25 or 500 μg of DNP-conjugated human serum albumin (HSA; Sigma-Aldrich)[27]. Then, the rectal temperature was measured for 120 min with an electronic thermometer (Physitemp Instruments). For PCA, mice were passively sensitized by intradermal injection with 30 ng of anti-DNP IgE. After 24 h, the mice were challenged by intravenous injection of 20 or 60 μg of DNP-HSA in saline containing Evans blue dye (Wako)[27]. Extravasation of blue dye in the ear was monitored for 30 min, and ear biopsies were incubated at 37 °C in 3 N KOH. Quantitative analysis of the extracts was performed by measuring the absorbance of blue dye at 620 nm. For active anaphylaxis, mice were immunized intraperitoneally on days 0 (day when OVA was first administered), 7 and 14 with 10 μg of chicken OVA (Sigma-Aldrich) in 100 μl of saline mixed with 200 μl of alum (Alu Gel S, which contained 2% $Al(OH)_3$; Serva). Seven days after the last immunization, the left and right ears of mice were injected intradermally with 30 μg of OVA. Net ear swelling was measured at 30 min after challenge with OVA.

Measurement of histamine and protease activities. The procedures were described previously[27]. Briefly, tissues were homogenized in PBS with a bead crusher (μT-01; Taitec) at 4 °C, and Triton X-100 was added to a final concentration of 0.5% (v/v). For the histamine assay, the lysates were treated with 3% (v/v) perchloric acid and left for 30 min on ice, and the resulting supernatants (tissue extracts) after centifugation at 10,000*g* for 30 min at 4 °C were applied to a cation-exchange WCX-1 column on HPLC (Shimadzu) to separate histamine, which was then measured fluorometrically by the *o*-phthalaldehyde method[45]. For the protease assay, 10 μl of the tissue extracts were diluted with 90 μl of 50 mM Tris-HCl (pH 8.3), followed by incubation with 20 μl of 1.8 mM chromogenic substrates for chymotrypsin- or trypsin-like proteases (S-2586 and S-2288, respectively; Chromogenix) and CPA (M-2245; Bachem) at 37 °C for 1–3 min. Changes in absorbance at 405 nm were measured.

Culture of mouse BMMCs and other bone marrow–derived cells. To prepare BMMCs, mouse bone marrow (BM) cells were cultured in IL-3–containing BMMC complete medium[27]. After 4–6 weeks of culture, >97% of the cells were identified as Kit$^+$FcεRIα$^+$ mast cells by flow cytometry. The coculture-driven maturation of immature BMMCs toward CTMC-like cells has been described previously[27]. Briefly, BMMCs were seeded onto Swiss 3T3 fibroblast monolayer and cocultured for the appropriate durations (typically for 4 d) in the presence of mouse SCF (100 ng/ml; Peprotech). The cells were trypsinized and reseeded in culture dishes, and nonadherent cells were collected. Purity (>99%) was confirmed by flow cytometry for Kit and FcεRIα. Maturation of BMMCs into CTMC-like cells was verified by staining their granules with alcian blue and counterstaining with safranin O. As required for experiments, 10 μM AT-56, 1 μM BW A868C, 10 μM BW 245C (Cayman Chemical) or 10 μM forskolin (Sigma-Aldrich) were added to the coculture.

BM cells were cultured with mouse granulocyte-macrophage colony stimulating factor (GM-CSF; 10 ng/ml; Peprotech) for 9 d, mouse macrophage colony stimulating factor (M-CSF; 100 ng/ml; Kyowa Kirin) for 3 d or mouse TSLP (1 μg/ml; R&D Systems) for 5 d in RPMI1640 medium (Invitrogen) containing 10% (v/v) FBS (Invitrogen) to obtain BMDCs, BMDMs or BM basophils, respectively[46,47]. The purity of each cell population was verified by flow cytometry for the expression of CD11c and MHC class II for BMDCs, the expression of F4/80 and CD11b for BMDMs, and the expression of FcεRIα and CD200R3 (or DX5α) coupled with a lack of expression of Kit for BM basophils (see below).

Activation of BMMCs. BMMCs (10^6 cells) before and after coculture with fibroblasts were sensitized with 1 μg/ml anti-DNP IgE for 2 h and then stimulated with various concentrations (typically 100 ng/ml) of DNP-BSA (Sigma-Aldrich), 100 ng/ml mouse SCF or 10 μg/ml C48/80 (Sigma-Aldrich). Degranulation was evaluated by measuring histamine or β-HEX release, as described previously[27]. The levels of eicosanoids were determined by ELISA in accordance with the manufacturer's instructions (Cayman Chemical). Expression of cytokines was assessed by real-time PCR. Lactate dehydrogenase activity was measured using an LDH Cytotoxicity Detection Kit (Takara).

Preparation and activation of mouse pMCs. To collect peritoneal cells, 5 ml of Hank's balanced salt solution (Invitrogen) was injected into the mouse peritoneal cavity, and the abdomen was massaged gently. After collecting peritoneal cells from the peritoneal fluid, they were resuspended in PIPES-buffered saline for electron microscopy or in BMMC-complete medium for degranulation assay. For degranulation, 10^6 cells were treated for 30 min with 1–5 μg/ml of human PLA2G3 or BV-PLA_2, with 1 μM A23187 (Sigma-Aldrich), or with 1 μg/ml anti-DNP IgE for 1 h and then with 100 ng/ml DNP-BSA for 30 min in the presence of 4 μM lysophosphatidylserine (Avanti Polar Lipids). The release of histamine was then evaluated.

Preparation of mouse skin mast cells and fibroblasts. Mouse ear skin was dispersed with 1.6 mg/ml collagenase type II (Worthington) and 0.1 mg/ml DNase I (Sigma-Aldrich) in RPMI1640 containing 10% FBS for 30 min at 37 °C and passed through a cell strainer (40-μm mesh size). Skin mast cells were identified as Kit$^+$FcεRIα$^+$ cells after CD45 gating by flow cytometry. The skin-dispersed cells were cultured in RPMI1640 containing 10% FBS, trypsinized and reseeded on culture dishes, and adherent cells grown to confluency were used as skin fibroblasts.

Preparation and culture of human mast cells and fibroblasts. Preparation and culture of mast cells from human skin and lung were performed as described previously[48]. Briefly, macroscopically normal human lung or skin tissue was obtained during surgery at the Nihon University Hospital under approval of the faculty ethics committee and informed consent from the patient. Lung and skin cells were dispersed from chopped lung and foreskin specimens by collagenase and hyaluronidase (Sigma-Aldrich). These cells were maintained for 6 weeks in MethoCult SF^{BIT} (Iscove's modified Dulbecco's medium (IMDM)-based serum-free medium containing 1.2% (w/v) methylcellulose;

doi:10.1038/ni.2586

Veritas) supplemented with human SCF (100 ng/ml; Peprotech) and human IL-6 (50 ng/ml; Peprotech). On day 42, methylcellulose was dissolved in PBS, and the cells were resuspended and cultured in IMDM medium (Invitrogen) containing 0.1% BSA, 100 ng/ml SCF and 50 ng/ml IL-6. The purity of human mast cells, as assessed with metachromatic staining, was more than 97%. Human skin and lung fibroblasts (CC-2511 and CC-2512, respectively) and their culture medium were purchased from Lonza. Human lung mast cells (5×10^5 cells) were seeded onto the human lung fibroblast monolayer and cocultured for 4 d in 500 µl of IMDM medium plus 2% FBS in the presence of SCF and IL-6, with medium change at 2-d intervals. The cells were trypsinized and reseeded in culture dishes, and nonadherent cells were collected. The purity of mast cells was normalized based on the expression of *KIT*.

Real-time PCR. Total RNA was extracted from tissues and cells using TRIzol reagent (Invitrogen). First-strand cDNA synthesis was performed using the High-Capacity cDNA Reverse-Transcriptase Kit (Applied Biosystems). PCRs were carried out using the TaqMan Gene Expression System (Applied Biosystems) on an ABI7700 Real-Time PCR system (Applied Biosystems). The probe-primer sets are listed in **Supplementary Table 2.**

Measurement of intracellular Ca^{2+} levels. Intracellular Ca^{2+} levels were measured as described previously[27]. Briefly, IgE-sensitized BMMCs on coverslips were loaded for 60 min with the fluorescent Ca^{2+} indicator fura-2/AM (5 µM; Invitrogen) in Tyrode-HEPES buffer (pH 7.4) containing 2.5 mM probenecid, 0.04% (v/v) pluronic acid and 1% (v/v) serum. Then, the cells were washed and stimulated with antigen. Fura-2 fluorescence images were obtained using an image analyzer (ARGUS-50; Hamamatsu Photonics) with excitation at 340 nm (F340) and 380 nm (F380) at 5-s intervals. The fluorescence ratio (F340/F380) was calculated using US National Institutes of Health ImageJ software.

Western blotting. Tissue homogenates (20 µg protein equivalent) or BMMCs (2×10^5 cells) were lysed in SDS-PAGE sample buffer (63 mM Tris-HCl (pH 6.8), 2% (w/v) SDS, 10% (v/v) glycerol, and 0.08% (w/v) bromophenol blue) containing 5% (v/v) 2-mercaptoethanol, and then subjected to SDS-PAGE. Proteins were subsequently blotted onto PVDF membranes (Bio-Rad), followed by blocking with 5% (w/v) milk powder in PBS containing 0.05% (v/v) Tween 20 (PBS-T). The membranes were probed with rabbit polyclonal antibodies to HDC[49], H-PGDS[30], Kit (18101; IBL), PLCγ2 (3872; Cell Signaling), phospho-PLCγ2 Y1217 (3871; Cell Signaling), $cPLA_2\alpha$ (2832; Cell Signaling) or phospho-$cPLA_2\alpha$ S505 (2831; Cell Signaling) or mouse monoclonal antibodies against Akt (D9E; Cell Signaling), phospho-Akt S473 (C67E7; Cell Signaling), ERK1/2 (MK12; BD Transduction Laboratories), phospho-ERK1/2 T202/Y204 (20A; BD Transduction Laboratories), JNK (37; BD Transduction Laboratories), phospho-JNK T183/Y185 (41; BD Transduction Laboratories), p38 (27; BD Transduction Laboratories) or phospho-p38 MAPK T180/Y182 (30; BD Transduction Laboratories) at 1:500–1:2,000 dilutions in PBS-T containing 1% (w/v) milk powder or in Can Get Signal Solution 1 (Toyobo) for 1.5 h. After membranes were washed, the membranes were incubated for 1 h with horseradish peroxidase (HRP)-conjugated anti-rabbit (AP156P; Chemicon) or anti-mouse (21040; Molecular Probes) IgG at 1:5,000 dilution in PBS-T containing 1% milk powder or in Can Get Signal Solution 2 (Toyobo), and then visualized with ECL Prime western blotting detection reagent (GE Healthcare Life Science) on LAS-4000 (Fuji Film).

Histological analysis. Ears were fixed in 10% (v/v) neutral buffered formalin, embedded in paraffin and cut using a microtome. The sections (4 µm thickness) were stained with 0.05% toluidine blue (pH 0.5) for the detection of mast cells. Degranulated mast cells were defined as those showing the release of cellular granules. For immunohistochemistry, sections were incubated in PBS containing 5% normal goat serum, 5% BSA and 0.025% Triton X-100 for 20 min and then immunostained with a rabbit polyclonal to human PLA2G3, which reacts with both mature human and mouse enzymes (whose homology is 83%)[22–24], and mouse L-PGDS[50], at dilutions of 1:200 and 1:1,000, respectively, in the same buffer at 4 °C overnight. These preparations were incubated with biotinylated goat anti-rabbit IgG (BA-1000; Vector Laboratories) in PBS containing 5% BSA, 0.025% Triton X-100 and 10% mouse serum for 30 min followed by incubation with avidin DH and biotinylated HRP (Vectastain ABC kit; Vector Laboratories). These preparations were stained with 0.5 mg/ml 3,3′-diaminobenzidine and 0.1% (v/v) hydrogen peroxide solution. Human tissue sections were obtained from Chiba University following approval by the faculty ethical committee and informed consent from the patient. For transmission microscopy, tissues or cells were fixed with 0.1 M sodium cacodylate buffer (pH 7.2) containing 1% (v/v) glutaraldehyde and 4% (w/v) paraformaldehyde, post-fixed with 2% (w/v) OsO_4 in PBS, dehydrated by a graded ethanol series, passed through propylene oxide and embedded in Poly/Bed812 EPON (Polyscience). Ultrathin sections (0.08-µm thickness) were stained with uranyl acetate and lead citrate and then examined using an electron microscope (H-7600; Hitachi).

Adoptive transfer of BMMCs into mast cell–deficient mice. BMMCs obtained from 8–12-week-old male mice were reconstituted by intradermal (10^6 cells) or intravenous (10^7 cells) injection into 6-week-old male $Kit^{W\text{-}sh/W\text{-}sh}$ mice. Six weeks after intradermal transfer or 12 weeks after intravenous transfer of BMMCs, the mice were subjected to IgE-Ag–induced PCA, as described above. Alternatively, mast cells from the base to the tip of the ears from these mice were evaluated by toluidine blue staining or by real-time PCR of mast cell marker genes.

Flow cytometry. Cells were stained with either a labeled monoclonal antibody or an isotype-matched control antibody (hamster IgG (HTK888), mouse IgG_1 (MOPC-21), rat IgG_{2a} (RTK2758) or rat IgG_{2b} (RTK4530); BioLegend) and analyzed by flow cytometry using FACSCalibur (BD Biosciences) or FACSAria III Cell Sorter (BD Biosciences) with FlowJo software (Tree Star). The antibodies used were specific for mouse Kit (2B8; BD Biosciences), FcεRIα (MAR-1; eBioscience), DX5 (DX5; eBioscience), CD200R3 (Ba13; BioLegend), CD45 (30-F11; eBioscience), CD11c (N418; eBioscience), MHC class II (M5/114.15.2; eBioscience), CD11b (M1/70; BioLegend), F4/80 (BM8; BioLegend), CD45R/B220 (RA3-6B2; BD Biosciences), CD3ε (145–2X11; eBioscience), Gr-1 (RB-8C5; BioLegend), FOXP3 (150D; BioLegend) and FR4 (12A5; BioLegend).

Microarray. Total RNA was extracted from BMMCs derived from $Pla2g3^{-/-}$ and $Pla2g3^{+/+}$ mice before and after coculture and purified using the RNeasy Mini Kit (Qiagen). The quality of RNA was assessed with a 2100 Bioanalyzer (Agilent Technologies). Both cDNA and cRNA were synthesized with a Low Input Quick Amp Labeling Kit according to the manufacturer's protocol (Agilent Technologies). Samples were hybridized to the Whole Mouse Genome Microarray Kit (4 × 44K; Agilent Technologies), washed and then scanned using a Laser Scanner GenePix 4000B (Molecular Devices). Microarray data were analyzed with Feature Extraction software (Agilent Technologies) and then imported into GeneSpringGX11.5 (Agilent Technologies). Probes were normalized by quantile normalization among all microarray data.

RNA interference. Swiss 3T3 fibroblasts were cultured in 12-well plates to 50% confluence and transfected with a Mission predesigned siRNA construct (20 nM) for *Ptgds* (SASI_Mm01_00116073 or 00116081; Sigma-Aldrich) or a scrambled control siRNA (Invitrogen) using oligofectamine (Invitrogen), according to the manufacturer's instructions. After 48 h, wild-type BMMCs were cocultured for 2 d with the transfected cells.

Electrospray ionization mass spectrometry (ESI-MS). ESI-MS lipidomics analysis using a 4000Q TRAP quadrupole-linear ion trap hybrid mass spectrometer (AB SCIEX) with an UltiMate 3000 nano/cap/micro-liquid chromatography system (Dionex Corporation) combined with an HTS PAL autosampler (CTC Analytics AG) was performed as described previously[44]. Briefly, phospholipids extracted from 10^7 BMMCs were subjected directly to ESI-MS analysis by flow injection; typically, 3 µl (3 nmol phosphorous equivalent) of sample was applied. The mobile phase composition was acetonitrile/methanol/water (v/v/v = 6/7/2) plus 0.1% (v/v) ammonium formate (pH 6.8) at a flow rate of 10 µl/min. The scan range of the instrument was set at m/z 200–1,000 at a scan speed of 1,000 Da/s. The trap fill-time was set at 3 ms in the positive ion mode and at 5 ms in the negative ion mode. The ion spray voltage was set at 5,500 V in the positive ion mode and at −4,500 V in the negative ion

mode. Nitrogen was used as a curtain gas (at a setting of 10 arbitrary units) and as a collision gas (set to 'high').

Statistical analysis. The Excel Statistical Program File ystat 2008 (Igaku Tosho Shuppan) was used to determine statistical significance evaluated by an unpaired Student's *t*-test for two groups or an analysis of variance (ANOVA) for multiple groups. *P* values of less than 0.05 and 0.01 were considered statistically significant. Data are presented as the mean ± s.e.m.

38. Satoh, T. *et al.* Prostaglandin D_2 plays an essential role in chronic allergic inflammation of the skin via CRTH2 receptor. *J. Immunol.* **177**, 2621–2629 (2006).
39. Segi, E. *et al.* Patent ductus arteriosus and neonatal death in prostaglandin receptor EP4-deficient mice. *Biochem. Biophys. Res. Commun.* **246**, 7–12 (1998).
40. Sugimoto, Y. *et al.* Failure of parturition in mice lacking the prostaglandin F receptor. *Science* **277**, 681–683 (1997).
41. Kobayashi, T. *et al.* Roles of thromboxane A_2 and prostacyclin in the development of atherosclerosis in *apoE*-deficient mice. *J. Clin. Invest.* **114**, 784–794 (2004).
42. Iizuka, Y. *et al.* Protective role of the leukotriene B_4 receptor BLT2 in murine inflammatory colitis. *FASEB J.* **24**, 4678–4690 (2010).
43. Sun, D. & Funk, C.D. Disruption of 12/15-lipoxygenase expression in peritoneal macrophages. Enhanced utilization of the 5-lipoxygenase pathway and diminished oxidation of low density lipoprotein. *J. Biol. Chem.* **271**, 24055–24062 (1996).
44. Ueno, N. *et al.* Analysis of two major intracellular phospholipases A_2 (PLA_2) in mast cells reveals crucial contribution of cytosolic $PLA_2\alpha$, not Ca^{2+}-independent $PLA_2\beta$, to lipid mobilization in proximal mast cells and distal fibroblasts. *J. Biol. Chem.* **286**, 37249–37263 (2011).
45. Shore, P.A., Burkhalter, A. & Cohn, V.H. Jr. A method for the fluorometric assay of histamine in tissues. *J. Pharmacol. Exp. Ther.* **127**, 182–186 (1959).
46. Lutz, M.B. *et al.* An advanced culture method for generating large quantities of highly pure dendritic cells from mouse bone marrow. *J. Immunol. Methods* **223**, 77–92 (1999).
47. Siracusa, M.C. *et al.* TSLP promotes interleukin-3-independent basophil haematopoiesis and type 2 inflammation. *Nature* **477**, 229–233 (2011).
48. Kajiwara, N. *et al.* Activation of human mast cells through the platelet-activating factor receptor. *J. Allergy Clin. Immunol.* **125**, 1137–1145 (2010).
49. Tanaka, S. *et al.* Expression of l-histidine decarboxylase in granules of elicited mouse polymorphonuclear leukocytes. *Eur. J. Immunol.* **34**, 1472–1482 (2004).
50. Gerena, R.L., Eguchi, N., Urade, Y. & Killian, G.J. Stage and region-specific localization of lipocalin-type prostaglandin D synthase in the adult murine testis and epididymis. *J. Androl.* **21**, 848–854 (2000).

doi:10.1038/ni.2586

DECREASED SURFACE SIALIC ACID CONTENT IS A SENSITIVE INDICATOR OF MUSCLE DAMAGE

YUKO IWATA, PhD,[1] OSAMU SUZUKI, PhD,[2] and SHIGEO WAKABAYASHI, PhD[1]

[1] Department of Molecular Physiology, National Cerebral and Cardiovascular Center Research Institute, Fujishiro-dai 5-7, Suita, Osaka 565-8565, Japan

[2] Laboratory of Animal Models for Human Diseases, National Institute of Biomedical Innovation, Ibaraki, Osaka, Japan

Accepted 12 August 2012

ABSTRACT: *Introduction*: The glycosylation state of the muscle sarcolemma is crucial for membrane strength and is thereby linked to pathologic conditions. No markers currently exist with sufficient sensitivity to detect muscle damage in biopsy samples. We aimed to determine whether surface sialic acid content is a useful criterion for estimating muscle injury. *Methods*: Sialic acid content was measured by comparing the fluorescence intensity of muscle sections stained with 2 types of lectins. One binds specifically to nonsialylated sugars, and the other binds to both sialylated and nonsialylated sugars. *Results*: Sialic acid levels were markedly reduced (60–80%) in muscles from dystrophin-defective mice, δ-sarcoglycan–deficient hamsters, merosin-deficient mice, and patients with muscular dystrophy, when compared with their healthy counterparts. *Conclusions*: Testing for a marked decrease in sialic acid levels, which is caused by the release of trace amounts of sialidase from damaged muscles, is a sensitive detection method for muscle injury and could be commonly utilized for various subtypes of muscular dystrophy.

Muscle Nerve **47:** 372–378, 2013

Muscular dystrophy is a severe degenerative disorder of skeletal muscle, characterized by progressive muscle weakness.[1] One subgroup of this disease is caused by a defect in the genes that encode for the components of the dystrophin–glycoprotein complex (DGC). This multi-subunit complex spans the sarcolemma to structurally link extracellular matrix proteins, such as laminin, to the actin cytoskeleton, thereby providing mechanical strength to muscle cell membranes.[2,3] Therefore, defects of the DGC result in marked disruption of membrane integrity and/or stability. Sarcolemmal damage accelerates the release of cytoplasmic enzymes or the entry of extracellular substances across the cell membranes. To date, increased serum creatine kinase (CK)[4] levels have been used as an indicator of the extent of muscle damage in patients with Duchenne muscular dystrophy or in corresponding animal models such as dystrophin-deficient mice (*mdx*). However, measurement of serum CK levels is not always a reliable indicator of muscle damage, because they rise and fall rapidly and are easily affected by stresses to the body from surgical procedures, vigorous exercise, or deep intramuscular injections.[5–7] In addition, other cytosolic enzymes released in serum, such as myoglobin, aldolase, or lactate dehydrogenase, have similar limitations with regard to the detection of muscle damage. Furthermore, merosin-deficient mice (*dy/dy*), another dystrophic model representative of human merosin-deficient congenital muscular dystrophy, demonstrated no detectable increase in serum CK levels despite their severe clinical phenotype.[8] Enhanced uptake of externally added Evans blue dye (EBD)[8] as a marker of membrane integrity cannot be used in humans owing to its toxicity; even in animals only postmortem muscle imaging is possible using EBD.

Establishing a diagnosis of muscle damage using biopsy samples and routine analysis is time consuming, even in distinguishing between myopathy and neuropathy. Therefore, newer and simpler methods would be useful for easy detection of muscle damage in various types of muscle degenerative disorders, and the validation of a new diagnostic marker would be invaluable.

Glycosylation has been demonstrated to be intimately linked to muscular dystrophy. Indeed, glycosylation of α-dystroglycan (α-dystroglycan DG), an essential component of the DGC, is critical for its interaction with the extracellular matrix to preserve the mechanical strength of the sarcolemma. Moreover, α-DG interacts with extracellular matrix proteins such as laminin through *O*-mannosyl–linked sialylated tetrasaccharides.[9–11] Abnormal glycosylation of α-DG has been detected in multiple forms of muscular dystrophy in mice and humans.[12,13] Therefore, we hypothesized that a test for changes in glycosylation of the sarcolemma could be used for diagnostic purposes for various types of muscular dystrophy.

Sialic acid (a generic term for neuraminic acid derivatives) is an important carbohydrate expressed on the terminal ends of glycan structures in many cell surface glycoproteins and glycolipids, where they mediate various cellular functions (e.g., cell–cell or cell–matrix interactions)[14] and are essential for mammalian survival, development, and growth.[15,16] Sialic acids are ultimately

Abbreviations: ACL, *Amaranthus caudatus* lectin; α-DG, α-dystroglycan; CK, creatine phosphokinase; DAPI, 4′,6-diamidino-2-phenylindole dihydrochloride; DGC, dystrophin–glycoprotein complex; *dy/dy*, merosin-deficient mice; EBD, Evans blue dye; FITC, fluorescein isothiocyanate; Galβ1,3GalNAc, galactose-(β1,3)-*N*-acetylgalactosamine; J2N-k, δ-sarcoglycan–deficient hamsters; J2N-n, control hamsters; *mdx*, dystrophin-deficient mice; PNA, peanut agglutinin; RT, room temperature; WT, wild-type

Key words: lectin staining, muscle injury, muscular dystrophy, sialic acid, sialidase

Correspondence to: Y. Iwata; e-mail: yukoiwat@ri.ncvc.go.jp

Published online 16 August 2012 in Wiley Online Library (wileyonlinelibrary.com). DOI 10.1002/mus.23632

transferred to oligosaccharide chains by the catalytic function of a large family of sialyltransferase enzymes. Conversely, the removal of sialic acid moieties is catalyzed by sialidase. The cytosolic fraction of skeletal muscles exhibits a higher level of sialidase activity than do other tissues.[17] Therefore, if sialidase is released from damaged muscle, it would greatly affect biological processes by changing the conformation of glycoproteins and uncovering or masking the binding sites of functional glycomolecules. Conversely, in distal myopathy with rimmed vacuoles (hereditary inclusion body myopathy), mutation of genes involved in the biosynthesis of sialic acids has been reported.[18–20] These findings raise the possibility that reduction in sialic acid levels has important pathological significance and may also be exploited as a sensitive detection method to monitor release of sialidase in various types of muscle degenerative disorders.

In this study, we addressed whether surface sialic acid content could be altered in muscular dystrophy.

METHODS

Materials. Biotinylated peanut agglutinin (PNA) lectin, *Amaranthus caudatus* lectin (ACL), and fluorescein isothiocyanate (FITC-avidin D; Vector Laboratories, Burlingame, California) were used according to manufacturer's instructions. The sialidase used was isolated from *Clostridium perfringens* (Sigma Chemical Co., St. Louis, Missouri). Alexa Fluor 647 goat anti-mouse IgG (H+L; Invitrogen, Carlsbad, California) and FITC-PNA (Vector Laboratories) were also used in several experiments.

Animals. Delta (δ)-sarcoglycan–deficient hamsters (J2N-k), a model of human δ-sarcoglycanopathy, and age-matched control hamsters (J2N-n) were purchased from Japan SLC, Inc. (Shizuoka, Japan). Four-week-old *dy/dy* and *mdx* mice and age-matched controls (wild-type [WT]) were purchased from the Jackson Laboratories (Bar Harbor, Maine). All animal experiments were performed in accordance with the animal experimentation guidelines of the National Cerebral and Cardiovascular Center (NCVC), Japan.

Human Tissues. Tissue samples were obtained from skeletal muscle biopsy specimens from the NCVC from patients with muscular dystrophy and by autopsies of patients without muscle failure as controls.[21] Written informed consent was obtained from all subjects.

Staining of Skeletal Muscle Sections with Lectins. The sugar chain properties in frozen sections (approximately 5–6 μm) of skeletal muscles were analyzed by the binding of biotinylated PNA or ACL, as described previously.[22] Frozen sections were fixed in 100% ethanol for 10 min at room temperature (RT). After washing with phosphate-buffered saline, the sections were incubated with each biotinylated lectin (10 μg/ml) for 15 min at RT. When sialidase treatment was performed, the sections were treated with 0–5000 mU of sialidase in 50 mM sodium acetate (pH 5) for 2 hours at 37°C before incubation with lectins. These lectins were visualized by incubating the sections with 20 μg/ml of FITC-avidin D for 5 min at RT, followed by observation under a fluorescence microscope (IX81; Olympus, Tokyo, Japan) equipped with confocal capability (Fluoview FV1000; Olympus). For greater time savings, the fixed sections were stained directly with FITC-PNA (10 μg/ml) for 15 min at RT. The nucleus was stained with 4′,6-diamidino-2-phenylindole dihydrochloride (DAPI; Dojindo Laboratories, Kamimashiki-gun, Japan).

Quantification of Fluorescent Intensity Visualized with Lectin Staining. Images of serial sections stained with lectins were analyzed by investigators blinded to the genotypes, using NIH Image software. The entire region covering each fiber and the region covering only the intracellular space in cross-sections were selected visually, and their fluorescence intensities were measured. Fluorescence intensity corresponding to the sarcolemmal region was calculated by subtracting the intensity of the intracellular region from that of the total area. All data were expressed as mean ± standard deviation (SD) unless otherwise indicated. Differences between the groups were determined using the Student *t*-test. $P < 0.05$ was considered statistically significant.

RESULTS

To specifically detect the sialylated sugar group, 2 types of lectins, PNA and ACL, were used. The PNA lectin specifically binds to nonsialylated galactose-(β1,3)-*N*-acetylgalactosamine (Galβ1,3GalNAc) moieties on oligosaccharide groups on glycoproteins or glycolipids, but not to sialylated sugar moieties (Fig. 1A). By contrast, ACL interacts with sialylated and nonsialylated forms of Galβ1,3GalNAc structures (Fig. 1A). Therefore, the amount of sialylated sugars can be measured easily by comparative staining between PNA and ACL in the plasma membrane (Fig. 1A). This strategy was applied to skeletal muscles from J2N-k and J2N-n hamsters. Skeletal muscles from both types of hamster were well stained with ACL (Fig. 1B and C), indicating that both types of sarcolemma express similar apparent levels of Galβ1,3GalNAc. By contrast, the

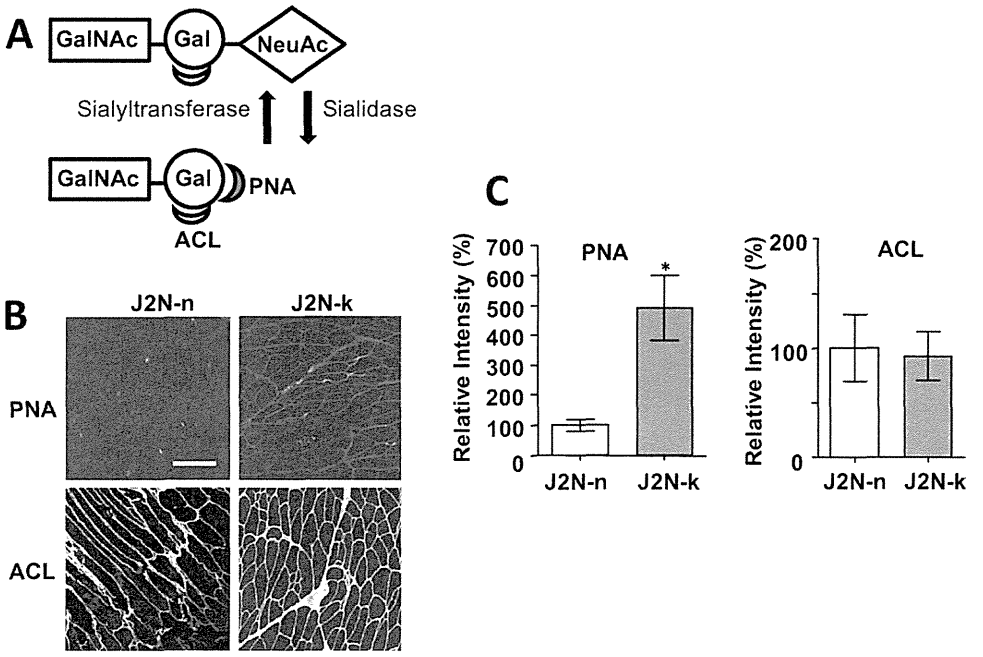

FIGURE 1. Increased PNA staining of J2N-k hamster muscles. (**A**) Schematic drawing representing the sialic acid–dependent or sialic acid–independent interaction of 2 types of lectins. Whereas ACL recognizes sialylated and nonsialylated sugars, PNA recognizes only nonsialylated sugars. NeuAc, neuraminic acid; Gal, D-galactose; GalNAc, *N*-acetyl-D-galactosamine. (**B**) Typical staining images with PNA or ACL. Frozen sections of quadriceps femoris muscle from dystrophic (J2N-k) and control hamsters (J2N-n) were stained with biotinylated PNA or ACL followed by FITC-avidin D. Scale bars: 50 μm. (**C**) Immunofluorescence images of myofiber cross-sections stained with lectins were analyzed by imaging software. Fluorescence intensity of each lectin staining was measured from 3 or 4 cross-sectional views of myofibers from 3 or 4 animals per group. Data were normalized with fluorescence in the J2N-n hamsters for each lectin. The data are presented as mean ± SD (n = 30–50 fibers/group). *$P < 0.05$.

sarcolemmas from the J2N-k hamsters were more extensively stained with PNA compared with those from the J2N-n hamsters (Fig. 1B); the intensity of staining with PNA was approximately fivefold greater in the former than in the latter (Fig. 1C), indicating that the sarcolemmas from the J2N-k hamsters contained higher levels of nonsialylated sugars.

Stronger staining with PNA was also observed in muscle sections of *mdx* mice (Fig. 2A), with a PNA staining intensity that was approximately sixfold greater than that in the WT mice (Fig. 2B). Furthermore, when this staining method was applied to *dy/dy* mice, considerable staining with PNA was observed in the muscle sections (Fig. 2C); the staining intensity with PNA was approximately fourfold greater in *dy/dy* than in WT mice (Fig. 2D).

An important question is whether increased PNA staining occurs in necrotic fibers alone or throughout dystrophic muscles, which include normal and regenerating fibers. Intracellular IgG in the necrotic fibers was stained with anti-IgG antibody, as described previously,[8] whereas regenerating fibers with central nuclei were stained with DAPI. Intense PNA staining occurred everywhere in the *mdx* muscles (Fig. 3), including IgG-positive necrotic fibers, regenerating fibers with central nuclei, and normal fibers without central nuclei (see merged image in Fig. 3).

We applied the aforementioned staining procedure to the muscle biopsy samples from patients with muscular dystrophy (Fig. 4A and B). Whereas faint staining with PNA was observed in normal control muscles, muscle samples from patients with muscular dystrophy (Becker and/or limb-girdle muscular dystrophy) were strongly stained with PNA (Fig. 4A); the staining intensity with PNA was more than fourfold greater in muscles from patients with muscular dystrophy than in normal muscles (Fig. 4B). These data suggest that, similar to dystrophic animal models, muscle samples from patients with muscular dystrophy possess markedly reduced levels of sialic acids.

Muscular dystrophy results in sarcolemmal damage, which accelerates the release of cytosolic enzymes into the extracellular space. Therefore, it is probable that a sufficient amount of sialidase is released from injured muscles to remove sialic acids from the sarcolemma. To measure the catalytic action of sialidase, frozen sections of skeletal muscles from healthy mice were treated with externally added sialidase and subsequently stained with PNA. Sialidase treatment resulted in extensive staining of the muscle surface with PNA (Fig. 5A)